A NEW ORGANIC ACID TO STIMULATE DEEP WELLS IN CARBONATE RESERVOIRS

A Thesis

by

AHMAD F. AL-DOURI

Submitted to the Office of Graduate and Professional Studies of
Texas A&M University
in partial fulfillment of the requirements for the degree of

MASTER OF SCIENCE

Chair of Committee,	Hisham A. Nasr-El-Din
Committee Members,	Robert Lane
	Mahmoud El-Halwagi
Head of Department,	A. Daniel Hill

May 2014

Major Subject: Petroleum Engineering

ABSTRACT

Carbonate acidizing has been carried out using HCl-based stimulation fluids for decades. However, at high temperatures, HCl does not produce acceptable results because of its fast reaction, acid penetration, and hence surface dissolution, and its high corrosion rate. As a result, alternatives to HCl have been investigated including organic acids. In this work, the reaction of a new organic acid with calcite was investigated using the rotating disk apparatus and coreflood setup. The organic acid was obtained using both a phosphorous-based and iron-based catalyst.

The rate of reaction of a 10 wt% solution of the new organic acid was measured using the rotating disk apparatus at temperatures up to 250°F. Low-permeability Indiana limestone (1-5 md) samples of 1.5 in. diameter and 0.75 in. length were used. The effect of disk rotational speed (100-1,500 rpm) was investigated. Samples of the reacted fluid were collected periodically and calcium and iron concentrations were measured using Inductively-Coupled Plasma, and used to determine the acid-rock reaction rate and to study the possibility of precipitation. Also, coreflood experiments at different injection rates and a temperature of 300°F were performed to study the effect of the acid on wormhole propagation in calcite. Low-permeability Indiana limestone (1-10 md) cores used in these experiments have a diameter of 1.5-in. and a length of 6 in.

For the phosphorus-based acid, experimental results showed that the rate of calcite dissolution at 205°F was controlled only by the rate of mass transfer of the acid to the surface. However, at 250°F, the reaction was controlled by both mass transfer and by the kinetics of the surface reaction. At 205°F, the reaction rate varied from 7.79E-07 to

4.47E-06 gmol/cm^2.s, while at 250°F, the range was between 5.82E-07 and 2.72E-06 gmol/cm^2.s. In coreflood experiments, the phosphorus-based acid caused calcium phosphate precipitation at 300°F, while the iron-based acid achieved breakthrough. Also, the optimum injection rate of the iron-based acid was determined to be 2.0 cm^3/min. This study summarizes the results obtained and recommends the use of the new organic acid for field applications in calcite reservoirs.

DEDICATION

This work is dedicated to my parents, Firas Al-Douri and Zaineb Abdullah, for their continued love and support.

Also, for my two brothers, Abdulhamid and Omar, for being the best brothers anyone can have.

ACKNOWLEDGEMENTS

I would like to thank my committee chair, Dr. Hisham Nasr-El-Din, and my committee members, Dr. Robert Lane, Dr. Mahmoud El-Halwagi, for their guidance and support throughout the course of this research.

Also, thanks to my mother, father, and brothers for their encouragement, patience, and love. My parents' constant support and care is what made me the person I am today.

Finally, thanks also go to my friends and colleagues and the Petroleum Engineering Department faculty and staff for making my time at Texas A&M University a great experience. I also want to extend my gratitude to the PFP Technology®, for providing partial financial support for this project.

NOMENCLATURE

A_0	=	Initial disk surface area, cm^2
C_b	=	Reactant concentration in the bulk solution, $gmol/cm^3$
C_s	=	Reactant concentration at the surface, $gmol/cm^3$
d[Ca]/dt	=	Calcium dissolution rate, $gmol/(cm^2.s)$
D	=	Diffusivity, cm_2/s
E_a	=	Reaction activation energy, kcal/gmol
$[H_b^+]$	=	Acid concentration in the bulk solution, $gmol/cm^3$
J	=	Mass flux, $gmol/(cm^2.s)$
K_a	=	Dissociation constant, M
K_m	=	Reactant mass transfer coefficient, cm/s
k_0	=	Pre-exponential factor, $gmol^{(1-m)}.cm^{(3m-2)}.s^{-1}$
k_0	=	Reaction rate constant, $gmol^{(1-m)}.cm^{(3m-2)}.s^{-1}$
m	=	Reaction rate order
M_A	=	Molarity of acid, M (gmol/L)
M_B	=	Molarity of base, M (gmol/L)
N	=	K/ρ, $cm^2.s(1/n^2)$
R	=	Rate of reaction, $gmol/(cm^2.s)$
R_d	=	Initial calcium dissolution rate, $gmol/(cm^2.s)$
Sc	=	Schmidt number
Sh	=	Sherwood number
t	=	Time, s

v	=	kinematic viscosity, mm^2/s
V_A	=	Volume of acid, mL
V_B	=	Volume of base, mL
ρ	=	Density, g/cm^3
ω	=	Frequence, Hz
Ω	=	Disk rotational speed, s^{-1}
r_s	=	Radius of disk, cm
$\emptyset'(n)$	=	Function depends on n

TABLE OF CONTENTS

Page

LIST OF FIGURES

Page

LIST OF TABLES

Page

CHAPTER I

INTRODUCTION AND LITERATURE REVIEW

Carbonate acidizing has been carried out using hydrochloric acid (HCl)-based stimulation fluids for decades (Nierode and Williams, 1971; Lund et al. 1973; Lund et al. 1975; AlKattan et al. 1998). However, at high temperatures, HCl does not produce acceptable stimulation results due to the following factors: fast reaction in the near-wellbore region, low acid penetration, and surface dissolution. As a result, many alternatives to HCl have been investigated including organic acids, chemically retarded acids (e.g. emulsified acids), and foamed acids. Organic acids have been used to stimulate carbonate reservoirs for more than four decades (Harris, 1961; Chatelain et al. 1976; Crowe et al. 1988; Fredd and Fogler, 1998a,b,c; Fredd, 2000; Huang et al. 2000; Nasr-El-Din et al. 2001). The two main organic acids that are frequently used to stimulate carbonate reservoirs are formic acid (HCOOH) and acetic acid (CH_3COOH), both of which are less reactive with carbonate rocks than hydrochloric acid (Nierode and Williams, 1971). In addition, acetic acid can be inhibited against all types of steel at elevated temperatures for extended periods of time (Harris, 1961). It is mostly used in high temperature reservoirs, where the fast HCl spending rate can cause severe tubing corrosion and poorly etched fractures (Crowe et al. 1988).

Nierode and Williams (1971) suggested that the lower rate of dissolution of calcite with organic acids was due to limitations associated with the kinetics of the surface reaction, while Chatelain et al. (1976) demonstrated that the dissolution process was influenced by the thermodynamics of the reversible reactions. Buijse (2004) developed a

new model for acid/calcite spending applicable to both strong and weak acids and to acid mixtures. A mixture of acetic and formic acids has been used to stimulate high-temperature/pressure wells in the Arun limestone field in Indonesia (Van Domelen and Jennings, 1995) and an economic comparison between HCl and organic acid blends was made. The base cost of an organic acid blend was determined to be higher than that of HCl; however, reductions in inhibition and gelling costs resulted in a final acid blend that was both technically and economically more attractive than an HCl-based system. A mixture of 7 wt% hydrofluoric acid (HF) and 5 wt% acetic acid (HAc) was used to remove calcium carbonate scales in gas wells in the Merluza field and was shown to be at least four times more efficient than 10 wt% HAc alone (Da Motta et al. 1998).

Citric acid is an alpha hydroxyl acid with three carboxylic and one hydroxyl groups. It has been used in oilfield treatments as an iron-control chemical in both carbonate and sandstone acidizing (Hall and Dill, 1988). Recently, citric acid has been used for carbonate stimulation by coating it with a layer of vegetable oil that prevents the acid from reacting with the formation until the capsules start melting at 150-180°F. This use of an encapsulated citric acid has produced mixed results in the field. Blauch et al. (2003) reported that the pressure and metal ions had a significant impact on whether calcium citrate forms and citric acid was shown to provide significant enhancement for matrix permeability. However, Burgos et al. (2004) reported no increase in production from the test well, possibly from the precipitation of calcium citrate. Al-Khaldi et al. (2007; 2005) used the rotating disk apparatus and coreflood tests to examine the reaction of citric acid and calcite. These studies indicated that the citric acid-calcite reaction was

hindered by the precipitation of calcium citrate on the surface and the impact of calcium citrate on core permeability diminished at pressures greater than 1,000 psi. In another study, Al-Khaldi et al. (2010) studied the effect of temperature on the diffusion coefficient of citric acid at a constant concentration and the behavior was found to follow Arrhenius law.

Lactic acid was used as an iron controlling agent, an alternative acid in acid fracturing, and for filter cake removal. Smith (1969) investigated different sequestration agents such as ethylenediaminetetraacetic acid (EDTA), nitrilotriacetic acid (NTA), citric acid, and lactic acid. The author recommended that lactic acid not be used at bottomhole temperatures greater than 100°F due to its inability to prevent ferric hydroxide precipitation at these temperatures. However, citric acid was found to be the most effective iron control agent because it was able to hold 3,000 ppm of iron (III) spent acid at temperatures up to 175°F.

In acid fracturing, two concerns are of particular importance. First, highly reactive acids such as HCl are consumed quickly by the reacting environment. This environment can be the filter cake layer, the face of the formation, or the formation in the immediate vicinity of the wellbore. As a result, acid penetration is shallow and the fracture conductivity does not improve much. The second concern is corrosion to iron-containing components such as casing, liners, coiled tubing, etc. As an alternative, organic acids can be used due to their lower reactivity. Still et al. (2007) introduced a method that can be applied to overcome these two problems: acids are pumped in a solid precursor form that

is hydrolyzed by water at the downhole conditions. The solid precursors include one or more of the following: cyclic dimers of lactic acid (lactide), solid form of polylactic acid (PLA), cyclic dimer of glycolic acid (glycolide), and a solid form of polyglycolic acid (PGA). The suggested acid concentration was between 0.83 to 2.5 ppg.

Lactic acid was also used, with other organic acids such as formic and acetic acids, as a filter cake removing agent. One of the methods introduced was to generate the acid in-situ by utilizing enzymes instead of the bacterial cells that were previously used (Almond et al. 1995). The system uses enzymes to catalyze the conversion of suitable substrates to generate organic acids in place. Recently, Al-Otaibi et al. (2006; 2008) used an ester as a precursor for lactic acid, which was determined to be more efficient than using precursors to other organic acids.

For acetic acid, Fredd and Fogler (1998c) investigated the kinetics of calcite dissolution in acetic acid solution over a wide range of pH using the rotating disk apparatus (RDA). The authors determined that at pH values below 2.9, dissolution is affected by both the rate of transport of reactants to the surface and the rate of transport of products away from the surface. This is due to the fact that the overall reaction is reversible. For pH values greater than 3.7, dissolution is affected by the kinetics of the surface reaction. Also, the authors introduced a surface dissociation mechanism involving water to describe calcite dissolution over a pH range of 8 to 14. The steps involved in this mechanism are: (1) adsorption of water onto the calcite surface, (2)

dissociation of adsorbed water, (3) surface reaction initiated by the dissociated hydrogen ions on the surface, and (4) desorption of calcium and carbonate products.

Fredd and Fogler (1998a; b) were the first authors to demonstrate the use of calcium chelating agents as stimulating fluids. They reported that EDTA can effectively form wormholes in limestone cores, even when injected at moderate and non-acidic pH (4-13) and at low flow rates where HCl is ineffective. EDTA solutions do not form sludge in acid-sensitive crude oils and are non-corrosive for alkaline solutions below 204°C. Fredd and Fogler (1998b) conducted a kinetics study of calcite dissolution with chelating agents using the RDA. The overall rate of dissolution was demonstrated to be influenced by the combined effects of hydrogen attack, chelating reactions, and the water reaction.

A new family of matrix stimulation fluids based on hydroxyaminocarboxylic acids chelating agents (HACA) was reported by Frenier et al. (2000; 2001a; b; 2003). These fluids can be used instead of EDTA, diethylene triamine pentaacetic acid **(**DTPA), or NTA because: (1) EDTA has limited solubility in acid when pH<4, (2) EDTA is not readily biodegradable, (3) NTA has a smaller stability constant for iron and calcium and is considered an animal carcinogen. Hydroxyethylenediaminetriacetic acid (HEDTA) has been demonstrated to be an efficient solvent for acidizing limestone cores over a wide range of pH at temperatures as high as 400°F (Frenier et al. 2001b). In addition, hydroxyethyliminodiacetate (HEIDA) salt was also developed for use as an oilfield stimulation fluid (Frenier et al. 2003). While HEIDA can be used in all of the

formulations requiring EDTA-type chelating agents, it has been determined to be more biodegradable than EDTA, HEDTA, and NTA.

Recently, polyaspartic acid (PASP), a readily biodegradable, non-toxic chelating agent, has been considered as a potential environmentally-friendly alternative to conventional agents for calcium salt dissolution. Burns (2002) studied the mechanism of calcite dissolution in the presence of polyaspartic acid using the RDA. PASP was treated as a ligand with four carboxyl groups according to the experimental titration data (Wu and Grant, 2002). Dissolution rates of calcite in PASP were evaluated as a function of pH, rotating speed, polymer concentration, and molecular weight. Results demonstrated that the dissolution is limited by mass transfer at low pH values and by interfacial reaction at high pH values. Also, at low pH values, dissolution proceeded by acid attack. In contrast, at high pH, dissolution occurred predominantly by a surface complexation mechanism.

Many experimental and theoretical studies have been performed in the past to understand reactive dissolution in carbonate reservoirs when acid is injected for stimulation purposes. Williams et al. (1979) recommended that acid injection is performed at the highest possible flow rate to avoid face dissolution near the wellbore. Daccord (1987) and Daccord et al. (1993a, b) performed experiments by injecting water into plaster. The dissolution of plaster with water led to the formation of patterns similar to those formed during dissolution of a porous medium caused by a chemical reaction. Lund et al. (1973; 1975) and Hoefner and Fogler (1989) conducted similar experiments

in limestone and dolomite cores by injecting HCl into linear cores. Bazin et al. (1995) conducted coreflow experiments on Estaillades, Savonierre, and Lavoux limesone and dolomite cores with a diameter of 50 mm and length 50 to 200 mm using 2M HCl at room temperature. Talbot and Gdanski (2008) presented a semi-empirical model on the dependence of pore volumes to breakthrough on acid concentration, system temperature, initial porosity and permeability, and core aspect ratio. The authors were able to collapse breakthrough curves from several laboratories using different conditions and rocks to a master curve. This allows for the prediction of optimum flow rate and acid volume required from a set of measured or controllable variables.

Several studies investigated the optimum conditions for wormhole formation during carbonate acidizing using HCl (Wang et al. 1993; Hill et al. 1995). They have shown that the dissolution pattern created can be characterized as being one of the following types: (1) compact or face dissolution in which most of the acid is spent near the rock face; (2) conical wormholes; (3) dominant wormholes; (4) ramified wormholes; and (5) uniform dissolution (Huang et al. 1997; Fredd, 2000). The transition from dissolution pattern 1 to 5 is commonly observed as the injection rate is increased. At low injection rates, the reactant is consumed on the inlet face of the core, resulting in face dissolution or complete dissolution of the core starting from the inlet injection face. The face-dissolution regime consumes large volumes of reactant and provides negligible penetration. At slightly higher injection rates, the treatment fluid can penetrate into the porous medium and enlarge injection channels. At intermediate injection rates, the acid is transported to the tip of the evolving injection channel, where subsequent consumption

propagates the channel and eventually leads to the formation of a dominant wormhole. At high injection rates, the dissolution channels become more highly branched or ramified as the fluid is forced into smaller pores. At very high injection rates, uniform dissolution is observed as the fluid is transported to most pores in the medium.

The type of dissolution structure was found to have a significant effect on the volume of acid required to obtain a given penetration depth. This effect was investigated by Fredd and Fogler (1998a; 1999). Fredd and Fogler (1999) studied the dependence of the number of PV to breakthrough (PV_{bt}) on the injection rate for the dissolution of Indiana limestone by various stimulation fluids, including DTPA, EDTA, acetic acid, and HCl. All of the fluids exhibit an optimum injection rate at which the number of PV required to breakthrough is the minimum and dominant wormhole channels are formed. Hence, the optimum injection rate represents the most effective conditions for matrix stimulation. The authors found these conditions at an optimum Damköhler number of 0.29. The number of PV to breakthough increases to the left and right of the minimum because of the formation of conical wormholes and ramified wormholes, respectively.

Huang et al. (1997) stated that the optimum acidizing conditions of a given formation can be determined by calculating the Damköhler number, given by **Eq. 1.1**:

$$N_{Da,opt} = \frac{(\frac{\pi}{20})^{3/2} r_{max}^3}{kL_p} \quad \text{.....(1.1)}$$

where $N_{Da,opt}$ is the optimum Damköhler number to form wormholes, r_{max} is the maximum pore radius, k is the matrix permeability, and L_p is the average pore length.

Huang et al. (2003) tested 10 wt% solutions of acetic acid, Na_4EDTA, and long-chain carboxylic acid (LCA) using Indiana limestone cores of 1 in. in diameter and 4 in. in length. These cores had a porosity of 15 vol% and a permeability of 2 to 3 md. The dissolving power of 10 wt% LCA was measured to be 0.45 lb/gal at room temperature. The authors performed the coreflood tests at 250°F using different injection rates to determine the optimum rate that will result in the minimum PV to breakthrough the core. All of the three chemicals used formed wormholes in the tested cores.

Wang et al. (2009) introduced a non-aggressive fluid to stimulate carbonate reservoirs. The fluid has a small corrosion rate compared to that of HCl, and because of its non-reactive nature, it can be used to stimulate heterogeneous reservoirs without using diverting agents. Parallel coreflood experiments showed that the fluid was able to stimulate both high- and low-permeability cores without using diverting agents.

GLDA, a chelating agent, was recently investigated by Mahmoud et al. (2010a, b) as a stan-dalone stimulation fluid. GLDA was able to stimulate calcite cores at different rates at temperatures up to 300°F. Mahmoud et al. (2011) studied the optimum injection rate of GLDA by performing coreflood tests using calcite cores of 6 and 20 in. in length and GLDA solutions with pH values of 1.7, 3, and 3.8. Parallel coreflood experiments showed that GLDA was able to stimulate cores with a low permeability contrast (up to 6.25). Also, the authors determined that the optimum injection rate was not affected by increasing from 180 to 300°F.

In this study, the reaction of a 10 wt% solution of a new organic acid with calcite will be examined under dynamic conditions. The objectives of this study are to: (1) examine the reaction of the new organic acid with calcite using RDA, (2) examine the effects of disk rotational speed and temperature on the reaction kinetics, (3) evaluate the ability of the new organic acid to create wormholes and hence enhance the permeability of limestone cores using the coreflood setup, (4) determine the potential for formation damage when the new organic acid is used to stimulate limestone cores at high temperatures, and (5) determine the optimum injection rate of the new organic acid in low-permeability Indiana limestone cores.

CHAPTER II

CHARACTERISTICS OF THE NEW ORGANIC ACID

Introduction

This investigation focuses on a new organic acid provided by PFP Technology®, an oilfield chemicals company based in Houston, TX. According to the description provided by the producers, the acid consists of three carboxylic acids, referred to as Proprietary Acids A, B, and C, mixed with glycerin.

The organic acid is derived from partial oxidation of lower molecular weight polyols. The polyol base is of a variable nature, due to being a side stream of a biomass conversion process. In addition, the polyol is composed of residual fatty acids, proteinaceous residues, phospholipids and monovalent inorganic salts. The variable nature of the polyol is controlled by the specific source of the biomass components and the subsequent manufacturing process. The mixed polyol is partially acid neutralized to a pH target from 4 to 5. This allows any non-water soluble acid residual to be removed by floatation. The remaining material is subjected to non-catalyzed oxidation by specific peroxide. The temperature is maintained below 70^{o}C for approximately 6 hours. The conversion is measured by acid base titration. The resulting material is a mixed organic acid that possesses an inherent increased viscosity and mineral dispersability when compared to typical organic acids.

The synthesis procedure was modified for the iron-based acid. In this process, a mixture of polyol and tap water were transferred into a glass reactor and a thermo couple and an external stirring system were also included. A catalyst system, comprised of a

mixture of hydrogen peroxide and iron (II) sulfate, was introduced and stirred. Then, the reactor was heated to 40°C allowing the iron (II) sulfate to oxidize by the following reaction:

$$H_2O_2 + Fe^{2+} \rightarrow H_2O + Fe^{3+} \quad \text{.....(2.1)}$$

In this reaction, the oxygen is reduced from -1 in H_2O_2 to -2 in H_2O and iron is oxidized from +2 to +3. During oxidation, samples were withdrawn at regular intervals and the pH was measured. As time accumulated, the pH decreased and more organic acids were formed. The end of the reaction is indicated by no change in the pH of the reaction mixture. Subsequently, heating is stopped and the product is removed from the reactor.

Experimental Studies

In order to characterize the new organic acid, several tests were performed to investigate its rheology. These tests included: pH, density, mass spectroscopy, ICP analysis of the acid's composition, and viscosity.

pH and Density Measurements

The pH of four samples of the new organic acid was measured using the pH meter in the Orion 950 Analytical Titrator. It was determined that the samples had an average pH value of 0.261. Using the Anton Paar DMA 35N density meter, the average density of these four samples was determined to be 1.123 g/cm³ at room temperature. In **Table 2.1** below, the pH and density results for each of the four samples is reported. From the data reported, it is clear that sample A is the most acidic of the four samples.

Table 2.1: pH and density measurements of four samples of the new organic acid.

Sample	Density, g/cm^3	pH
Sample A	1.075	0.59
Sample B	1.119	1.93
Sample C	1.151	1.84
Sample D	1.145	1.44

Mass Spectrometry

In order to perform the mass spectroscopy analysis of the acid, the Applied Biosystems 4800 TOF Analyzer spectrometer from the Texas A&M University Department of Chemistry was used. Samples A and D of the new organic acid were tested. To do so, both samples were reacted with acetic anhydride, shown below in **Fig. 2.1**, for one hour at 45°C and left to stand for 24 hours.

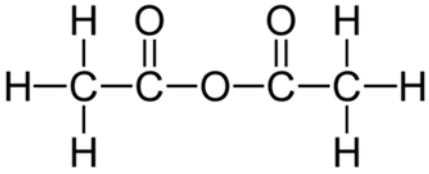

Fig. 2.1- Acetic anhydride.

Sample A had a higher amount of glycerol than sample D, indicated by the higher peak at m/z=92 amu at the same retention time. However, no definite structure or molecular weight was determined because of the viscosity of glycerol limited the number of ionization techniques that could be used in this analysis. Also, a large number

of alcohol and acid derivatives were detected in both samples, especially A, which made it very difficult to determine a molecular structure.

Analysis of Acid Composition

To determine the composition of the new organic acid, each of the four samples were analyzed using the Perkin-Elmer Inductively Coupled Plasma spectrometer. In order to calibrate the machine, a multi-element standard containing Al, Ca, Fe, Mg, and Si was used to indicate the elements that needed to be measured. From the results below in **Table 2.2**, it is clear that Ca and Fe are the two most plentiful elements in sample A new organic acid. Each of the samples A, B, and C had 150 mg of calcium (Ca) less than the original sample. Also, sample C had twice as much iron as the original sample.

Table 2.2: Acid composition analysis results.

	Concentration, mg/l			
Ion	**Original Sample (A)**	**Sample B**	**Sample C**	**Sample D**
Al	4.5	0.0	0.0	196.9
Ca	467.6	0.0	0.0	31.8
Fe	56.9	469.2	184.3	217.7
Mg	2.4	0.0	0.0	0.0
Si	5.6	0.0	0.0	0.0
P	11,960	25.8	14.3	0.0

Viscosity of New Organic Acid

The viscosities of samples A, C, and D, as received, and a 10 wt% solution of sample A were measured at room temperature using two different types of capillary viscometers. Since none of sample B was left, its viscosity could not be measured for this investigation.

For samples A and D, the viscosities were measured using an Ubbelohde PSL-ASTM-IP 1 capillary viscometer (viscosity range: 2-10 mm^2/s). The viscometer is calibrated according to the following equation:

$$v = 0.01045\ (\frac{mm^2/s}{s}) \times t(s) \quad \text{.....(2.2)}$$

For sample C, and the 10 wt% solution of sample A, the viscosity was measured using an Ubbelohde PSL-AST-IP 0C capillary viscometer (viscosity range: 1-5 mm^2/s). This viscometer is calibrated according to the following equation:

$$v = 0.003081\ (\frac{mm^2/s}{s}) \times t(s) \quad \text{.....(2.3)}$$

By measuring the time (in seconds) it takes for the fluid to travel the distance specified on the viscometer, the viscosity can be obtained using **Eqs. 2.2** and **2.3**, as appropriate for each sample.

Later in this study, the 10 wt% solution of samples A will be extensively used in the rotating disk apparatus study of this acid at temperatures of 150, 200, and 250°F. Thus, its viscosity will be measured at temperatures up to 50°C so that a correlation can be found between viscosity and temperature, as shown in **Fig. 2.2**. The measurements conducted on all the samples mentioned above are shown below in **Table 2.3**.

Table 2.3: Data for viscosity measurements of the new organic acid.

Sample	Temperature, °C	Time, seconds	Kinematic Viscosity, mm^2/s	Dynamic Viscosity, cP
A	25	329	3.438	3.937
C	25	1097	3.380	3.870
D	25	413	4.316	4.942
10 wt% A	25	369	1.13	1.215
10 wt% A	40	251	0.776	0.829
10 wt% A	45	231	0.712	0.759
10 wt% A	50	213	0.653	0.695
10 wt% D	25	367	1.15	1.317
10 wt% D	40	250	0.77	0.877
10 wt% D	45	252	0.714	0.811
10 wt% D	50	205	0.602	0.737

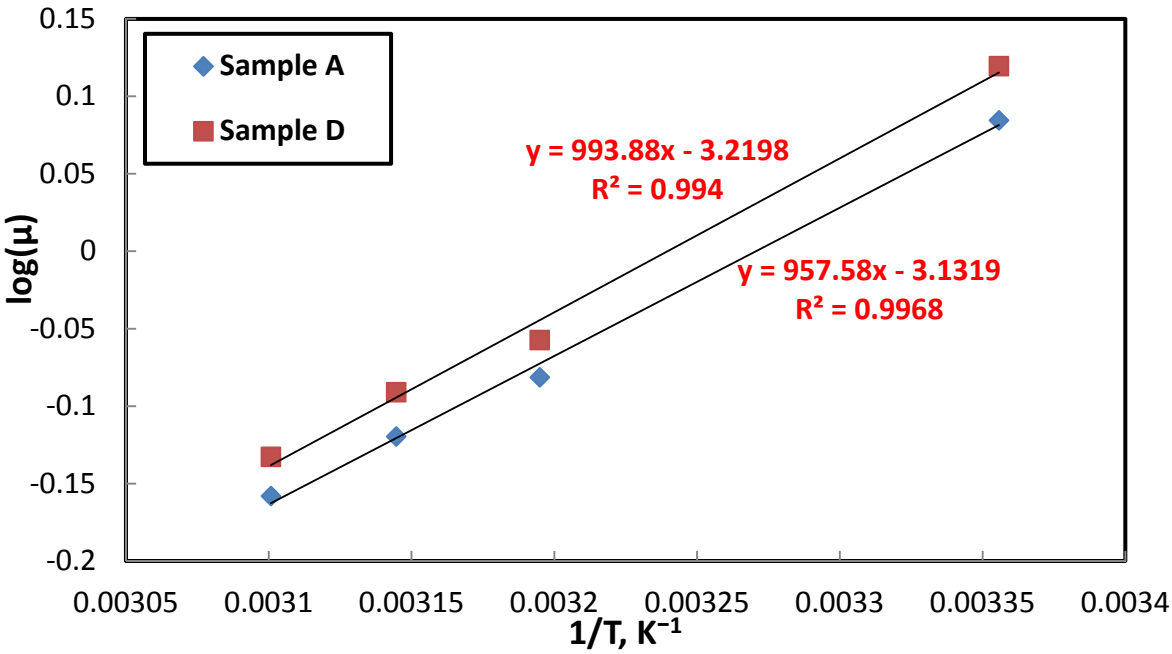

Fig. 2.2- Viscosity values of two 10 wt% solutions of the new organic acid as a function of temperature.

Titration of New Organic Acid (Samples A and D)

Since the known concentration of the acid samples was given as 50 wt%, it was essential to determine their molarities and molecular weights. To do so, a 10 wt% solution of each of samples A and D was titrated with a 2.0 M solution of NaOH. The reason for this choice was that most of the experiments conducted in this study were done using the two aforementioned samples. **Fig. 2.3** shows the titration curves for the two samples. Sample A is observed to have two equivalence points (4.75 mL and 7.0 mL of NaOH), while sample D has only one (9.0 mL).

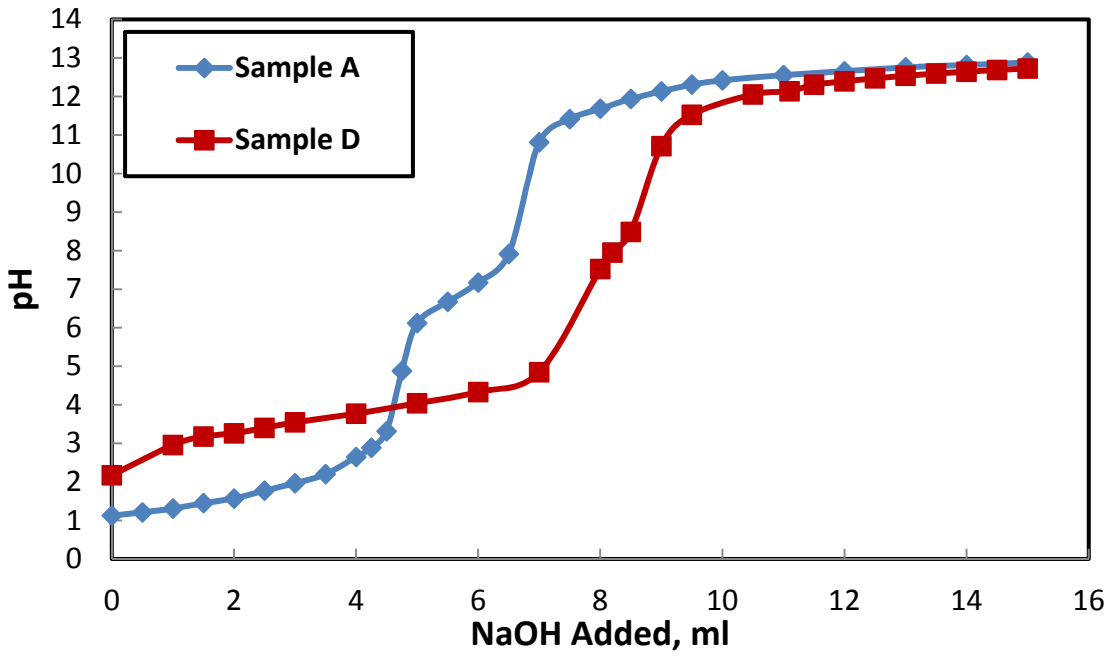

Fig. 2.3- Titration of samples A and D.

From the data obtained, the molarity of the acid can be calculated as follows:

$M_A V_A = M_B V_B$ ..... (2.4)

where M_A and M_B are the molarities of the acid and base, and V_A and V_B are the volumes

of the acid and base, respectively. Since 11.0 g of the acid were used from each sample, their respective densities were used to calculate the volume of acid used in each titration. The volume of base was the equivalence point, which is obtained by calculating the point with the highest change in slope from **Fig. 2.3**. Using **Eq. 2.1**, the molarity of sample A was calculated to be 1.324 M while sample D was determined to have a molarity of 1.874 M. After calculating the molarity of samples A and D, the molecular weight of each could be determined by the following equation:

$$Molarity\ \left(\frac{gmol}{cm^3}\right) = \left(\frac{wt\%\ of\ acid}{100}\right) \times \frac{Density\ (\frac{g}{cm^3})}{Molecular\ Weight\ (\frac{g}{gmol})} \quad \text{..... (2.5)}$$

Using the molarities obtained from the previous calculation, along with the density of each sample, the molecular weights of samples A and D were determined to be 392.86 g/gmol and 305.56 g/gmol, respectively. Since the reaction of sample A was run at a higher temperature than that of sample D (70°C compared to 40°C), it is reasonable that it has a higher molecular weight due to the possibility of runaway reactions occurring during the synthesis process. These reactions caused an elongation of the acid chain and thus, a higher molecular weight. This occurrence agrees with the findings of the mass spectrometry results, where the large number of alcohol and acid derivatives that were detected made the determination of a structure to be difficult.

Since sample A is a diprotic acid, it will yield two H^+ ions per acid molecule. Since its molecular formula is not known, a generic formula for the dissociation of a diprotic acid in water can be used as follows:

$$H_2X_{(aq)} \leftrightarrow H^+_{(aq)} + HX^-_{(aq)} \quad \text{.....(2.6)}$$

$HX^-_{(aq)} \leftrightarrow H^+_{(aq)} + X^{2-}_{(aq)}$……...(2.7)

The equations for the acid-base reactions occurring between sample A and sodium hydroxide, NaOH, are:

$H_2X + NaOH \rightarrow NaHX + H_2O$……...(2.8)

from the beginning to the first equivalence point. From the first to the second equivalence point, the equation is:

$NaHX + 2NaOH \rightarrow Na_2X + 2H_2O$……...……...……...(2.9)

Subsequently, the half-titration method can be used to determine the acid dissociation constants, K_{a1} and K_{a2}, for its two dissociations observed above. The K_a expressions are as follows:

$K_{a1} = \frac{[H^+][HX^-]}{[H_2X]}$……...(2.10)

$K_{a2} = \frac{[H^+][X^{2-}]}{[HX^-]}$……...(2.11)

The first half-titration point occurs when one-half of the H^+ ions in the first dissociation have been titrated with NaOH, so that $[H_2X]=[HX^-]$. This point is found by dividing the first equivalence point volume by two. Similarly, the second half-titration point occurs when one-half of the H^+ ions in the second dissociation have been titrated with NaOH, so that $[HX^-]=[X^{2-}]$. This point is midway between the first and second equivalence point volumes. For sample A, the first half-titration volume is (4.75 mL)/2=2.375 mL and the second half-titration volume is (4.75+7.0 mL)/2=5.875 mL. The pH values at the first and second half-titration volumes are 1.722 (pK_{a1}) and 7.045 (pK_{a2}), respectively. Using **Eq. 2.12** below, the dissociation constants K_{a1} and K_{a2} were determined to be 1.897×10^{-2}

M and 9.015×10^{-8} M.

$$K_a = 10^{-pK_a} \quad \text{.....(2.12)}$$

Conclusions

Four samples (A, B, C, and D) of a new organic acid were examined as effective fluids for matrix treatments in deep wells in carbonate reservoirs. Based on the results obtained, the following conclusions can be drawn:

1. Sample A was synthesized using phosphoric acid while samples B, C, and D used Fenton's reagent as a catalyst.
2. The density of the four samples ranged between 1.075 and 1.145 g/cm^3 and their pH ranged from 0.59 to 1.93. Sample A was the most acidic as it had the lowest pH value.
3. Mass spectrometry analysis on samples A and D indicated that glycerol was present in higher quantities in sample A but provided no conclusive evidence on its molecular structure/formula.
4. ICP analysis indicated the presence of approximately 12,000 ppm of phosphorus in sample A due to the use of phosphoric acid in the synthesis process, which will affect the reactivity of the acid at high temperatures.
5. The viscosity of the acid samples, as received, ranged between 3.38 and 4.32.
6. By titration with 2.0 M NaOH, sample A was found to be a diprotic acid while sample D was found to be a monoprotic acid.
7. From the titration results, the molecular weights of samples A and D were determined to be 392.86 g/gmol and 305.56 g/gmol, respectively.

CHAPTER III

KINETICS OF CALCITE DISSOLUTION IN A NEW ORGANIC ACID

Introduction

In the previous chapter, the rheological properties of the new organic acid were investigated. In this part of the study, the objectives are to: (1) examine the reaction of four samples (A-D) of the new organic acid with calcite using RDA, (2) examine the effects of disk rotational speed and temperature on the reaction rate, and (3) determine the diffusion coefficient of sample A in calcite.

Theory of the Rotating Disk Apparatus

In order to study the effects of one step on the overall reaction, it is important to eliminate the effects of the other steps. Therefore, kinetics of the surface reaction can be determined when the mass transport process is faster than the surface reaction. This case is known as surface reaction limited. On the other hand, if the diffusion to the surface is slower than the rate of surface reaction, the main resistance lies in the mass transfer boundary layer, and the reaction is called mass transfer limited. Levich (1962) introduced the mathematical description of the situation in which a molecule diffuses from the bulk solution of a fluid to the surface of a solid, and it is shown below in **Eq. 3.1**:

$$\frac{\partial C}{\partial t} + uC = D\,\nabla^2 C \qquad (3.1)$$

where *C* is the solute concentration, *u* is the velocity, and *D* is the solute diffusivity. The problem was solved analytically for different geometries such as parallel plates, a tubular reactor, and a disk rotating in a semi-infinite volume (Barron et al. 1962; Nierode and

Williams, 1971; Levich 1962; Newman 1966; Ellison 1969). Under laminar flow conditions ($Re<3*10^5$), Navier-Stokes equations for the three-dimensional flow system were solved. The mass transfer flux of solute to the solid surface can be determined as follows from **Eq. 3.2**:

$$J = k_m(C_b - C_s) \quad \text{(3.2)}$$

where J is the mass flux, k_m is the reactant mass transfer coefficient, and C_b and C_s are the solute concentration in the bulk solution and at the solid-liquid interface respectively. For non-Newtonian fluids, Hansford and Litt (1968) solved the convective diffusion equation and introduced modified Reynolds and Schmidt numbers to take into account the shear dependence of the viscosity power-law. The modified Reynolds and Schmidt numbers become:

$$Re = \frac{r_s^2 \omega^{2-n}}{N} \quad \text{(3.3)}$$

$$Sc = \frac{N\omega^{n-1}}{D} \quad \text{(3.4)}$$

where N is equal to (K/ρ), ρ is the fluid density, r is the disk radius, and D is the diffusivity. The final solution was introduced in the form of three dimensional groups Re, Sc, and Sh (Sherwood number), as shown in **Eq. 3.5**. The average mass flux to the solid surface can then be determined using **Eq. 3.6**:

$$Sh = \varphi'(n) Sc^{1/3} Re^{1/3[n+2/n+2]} \quad \text{(3.5)}$$

$$J = \frac{Sh\, D}{r}(C_b - C_s) \quad \text{(3.6)}$$

Values of ϕ'(n) as a function of n are given in **Table 3.1.** When **Eq. 3.5** is substituted in **Eq. 3.6** and Re and Sc numbers are replaced by their definitions from **Eqs. 3.3** and **3.4**, the average mass flux of a solute diffuses from the bulk of solution to the solid surface as a function of the disk rotating speed ω, bulk concentration C_b, diffusivity D, and the power-law parameters n and K can be obtained as follows:

$$J = [\varphi'(n)(\frac{K}{\rho})^{\frac{-1}{3(1+n)}}(r_s)^{\frac{(1-n)}{3(1+n)}}\left(\omega\omega^{\frac{1}{1+n}}D^{2/3}\right](C_b - C_s) = k_m(C_b - C_s)\text{.....(3.7)}$$

Table 3.1- Values of $\emptyset'(\boldsymbol{n})$ as a function of n (Hansford and Litt, 1968).

n	0.2	0.4	0.5	0.6	0.8	1	1.3
$\emptyset'(\boldsymbol{n})$	0.695	0.662	0.655	0.647	0.633	0.620	0.618

The term k_m is the mass transfer coefficient for non-Newtonian fluids rotating at the surface of semi-infinite disk. However, if the reactor vessel is at least twice the disk radius, the observed rate is independent of the vessel diameter. It is important to note that according to **Eq. 3.7**, the mass flux for non-Newtonian fluids is proportional to the disk rotational speed raised to the power 1/(1+n). In the case of a Newtonian fluid, n is equal to 1 and the rotational speed is raised to the power 0.5.

At low rotational speeds, the mass transfer of the reactant to the surface is remarkably slower than the surface reaction. As a result, the rate of reaction can be determined directly from the mass flux equation (**Eq. 3.7**). In this case, the reaction rate is proportional to the rotating speed raised to the power 1/(1+n). It is then acceptable to assume that the surface concentration will be much less than the bulk concentration and

for rapid surface reactions, it would be practically zero. Therefore, the rate of reaction R can be determined from **Eq. 3.8**:

$$R = [\varphi'(n)(\frac{K}{\rho})^{\frac{-1}{3(1+n)}}(r_s)^{\frac{(1-n)}{3(1+n)}}\left(\omega\omega^{\frac{1}{1+n}}D^{\frac{2}{3}}\right]C_b = A(\omega)^{\frac{1}{1+n}} \quad \text{.....(3.8)}$$

For a certain initial bulk concentration, plotting the initial rate of reaction versus the disk rotational speed to the power 1/(1+n) should yield a straight line with slope "A" that is proportional to the diffusivity raised to the power 2/3. Hansford and Litt (1968) stated that the results they obtained suggest that the mass transfer is reflecting the presence of three different flow regimes: reverse, toroidal, and centrifugal flow in which **Eq. 3.7** is only valid for the centrifugal regime.

At high rotational speeds, the mass transfer boundary layer decreases and as a result, the mass transfer decreases. The rate of reaction becomes controlled by the rate of reaction at the surface of the solid. In such cases, the rate of reaction is no longer proportional to the disk rotational speed and it should be obtained from the rate expression that describes the rate of reaction as a function of the reactant and product concentrations at the surface and the temperature of reaction. For solid-liquid reactions at the interface of the solid surface, progression of reaction does not change the amount of solid per unit volume of the solid. Therefore, the solid concentration becomes constant and is usually lumped into the reaction rate constant as in the case of the carbonate reaction with the new organic acid examined in this study. If the surface reaction is the rate limiting step, the mass transfer resistance is considered very small especially at high rotational speeds. Therefore, the acid concentration on the rock surface

is assumed to be equal to the acid concentration in the bulk concentration. The rate expression can then be written as a function of the acid bulk concentration by assuming a simple power law expression that was reported for HCl with calcite (Nierode and Williams, 1971; Lund et al. 1973; 1975; Taylor et al. 2004). The general expression can be formulated as follows, **Eq. 3.8**:

$$R = k_r[H_b^+]^m \quad (3.9)$$

where k_r is the reaction rate constant, $[H_b^+]$ is the acid concentration in the bulk solution, and m is the reaction rate order. The dependence of the reaction rate constant on temperature is described by the Arrhenius equation, shown below in **Eq. 3.9**:

$$k_r = k_0 e^{-E_a/RT} \quad (3.10)$$

where k_o is the pre-exponential factor, and E_a is the reaction activation energy. The plotting of log k_r (the reaction rate constant) versus the reciprocal of the absolute temperature yields a straight line that has a slope of $(-E_a/R)$.

Experimental Studies

Materials

Core samples from blocks of Indiana limestone were cut into disks with a diameter of 1.5 in. and a length of 0.75 in.. Samples were saturated in water, and the weight of the samples was measured before (dry) and after saturation. The average porosity was 17.22 vol%.

Acid Preparation

The new organic acid was obtained at an initial concentration of 50 wt%. For the experimental procedure, the acid was diluted to a concentration of 10 wt%. To do so, de-ionized water was obtained from a water purification system that has a resistivity of 18.2 MΩ.cm. Also, 0.1 vol% corrosion inhibitor (proprietary alkoxylated fatty amine salts, alkoxylated organic acid, Thiourea, N, N'-dibutyl) was added to prepare the acid.

Rotating Disk Apparatus

Reaction-rate experiments formed using a rotating-disk apparatus. Then, they were fixed in the disk-holder assembly into the reactor vessel using heat-shrinkable Teflon tubing. Reaction fluid was poured into the reservoir vessel, and both the vessel and fluid were heated to the desired temperature. Compressed N_2 gas was used to pressurize the reservoir vessel to a predetermined pressure that would be sufficient to transfer the acid to the reactor vessel resulting in a reactor pressure of 1,500 psig. A pressure greater than 1,000 psig is necessary in the reaction vessel to ensure that most of the evolved CO_2 is kept in solution and does not affect the system hydrodynamics and the dissolution rate (Lund et al. 1973; Fredd and Fogler, 1998c). The rotational speed was then set to the selected value, and the time is started at the moment at which the valve between the reservoir and the reactor vessel is opened.

Samples were withdrawn at equal intervals of 2 minute up to 20 minutes. The calcium concentration in the samples was measured using a Perkin-Elmer inductively-coupled plasma (ICP) spectrometer. The amount of calcium in the reaction vessel was then calculated and plotted vs. time. The slope of this line gives the rate of change in calcium

concentration over time (d[Ca]/dt)**.** Because of the change in the area of the disk, the initial surface area was used to determine the initial rate of calcite dissolution as follows:

$$R_d = \frac{1}{A_0}\frac{d[Ca]}{dt} \quad \text{.....(3.11)}$$

where R_d is the rate of dissolution, and A_0 is the initial surface area of the disk, taking into account the rock porosity.

Results and Discussion

Effect of Disk Rotational Speed on Calcium Concentration

The rate of calcite dissolution of a 10 wt% solution of the new organic acid was measured at rotational speeds between 100 and 1500 rpm at three different temperatures (150, 200, and 250°F) as shown in **Fig. 3.1** and summarized in **Table 3.2.** Since this acid is assumed to be a Newtonian fluid, n is assumed to be 1and the rotational speed is raised to 1/(1+1), or 0.5. At 150°F, the data showed a plateau for rotational speeds of 500-1500 rpm and the average dissolution rate in this range was 1.386E-06 gmol/cm^2.s. This behavior indicates that, at a temperature of 150°F, the rate of dissolution is controlled by mass transfer up to 500 rev/min. At higher rotational speeds (500-1,700 rev/min), the reaction of the new organic acid is mainly controlled by the kinetics of the surface reaction.

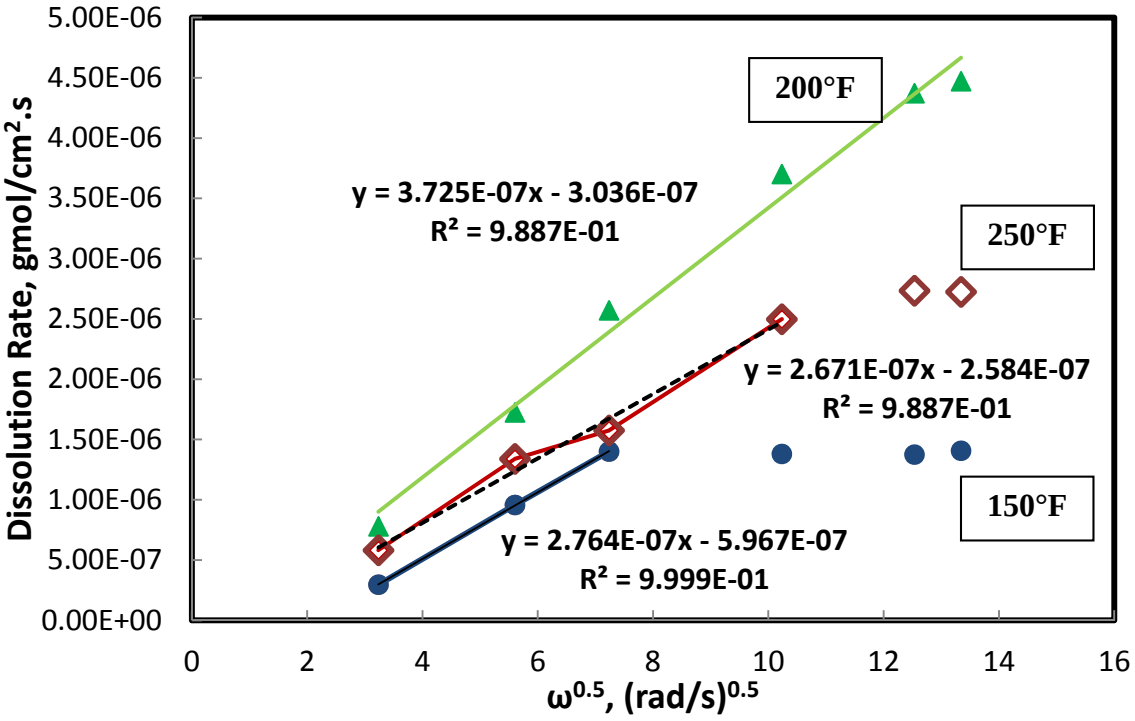

Fig. 3.1- Dissolution rate of Indiana limestone in 10 wt% new organic acid at 150, 200, and 250°F.

Table 3.2: Summary of reaction rate data for the sample A.

	Reaction Rate, gmol/cm^2.s		
Disk Rotational Speed, rpm	**150°F**	**200°F**	**250°F**
100	2.95909E-07	7.79249E-07	5.82067E-07
300	9.57632E-07	1.3867E-06	1.3398E-06
500	1.40073E-06	2.57148E-06	1.57515E-06
1000	1.38064E-06	3.70189E-06	2.49816E-06
1500	1.37553E-06	4.37123E-06	2.73459E-06
1700	1.40669E-06	4.47076E-06	2.72547E-06

In **Fig. 3.2,** the calcium concentration is shown as a function of time at a temperature of 150°F. Calcium concentrations of up to 2,500 mg/L were obtained at a

rotational speed of 1,000 rev/min. Also, from the figure, it is clear that the calcium concentrations were higher at 1,000 rev/min than they were at 1,500 rev/min. However, the slopes of both data sets were very similar, and as a result, both had essentially identical dissolution rates. This behavior confirms that at high rotational speeds (>500 rev/min), the reaction is controlled mainly by the surface reaction kinetics, as indicated above.

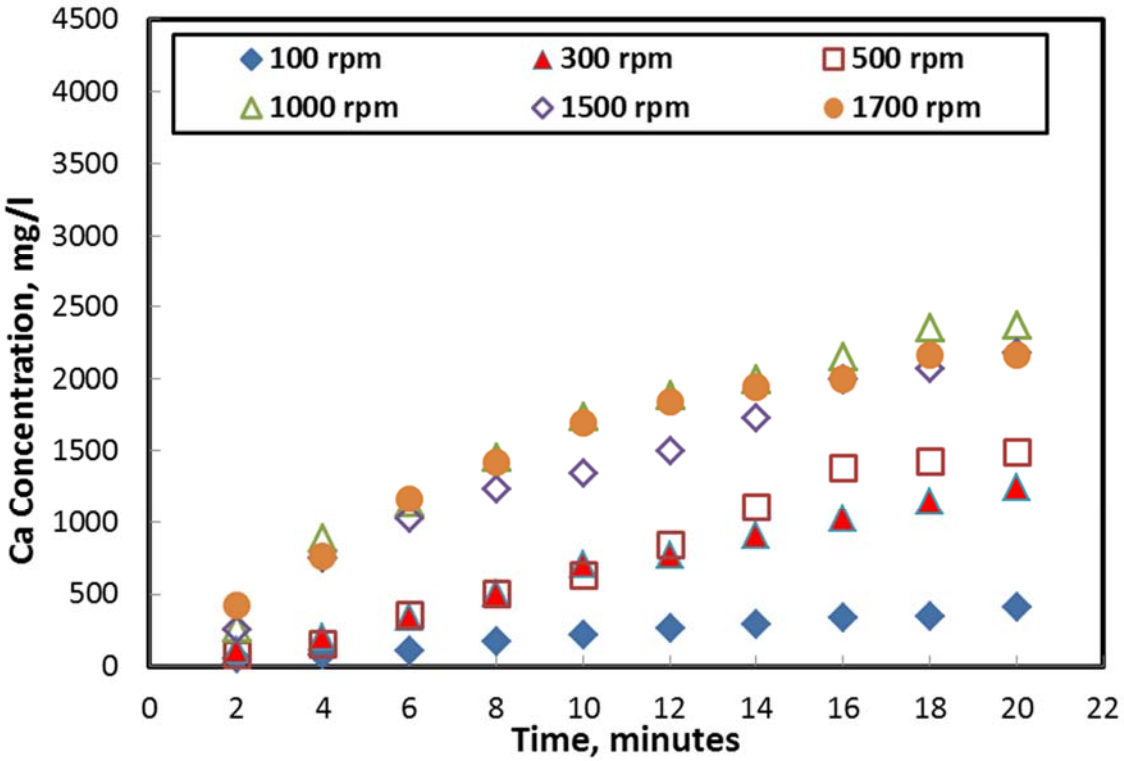

Fig. 3.2- Calcium concentration as a function of time for the reaction of a 10 wt% new organic acid with Indiana limestone at 150°F.

Increasing the temperature to 200°F showed that the dependence of the rate of dissolution on the disk rotational speed had increased and the data did not level off, or plateau, at any rotational speed. Alternatively, **Fig. 3.3** illustrates the change of the

concentration of the produced calcium with time for the reaction at 200°F. An increase in the calcium concentration was obtained for the reactions at 100-1500 rev/min, indicating that the dissolution of the new organic acid in Indiana limestone was fully dependent on the disk rotational speed. At a rotational speed of 1,500 rev/min, the calcium concentration reached as high as 4,000 mg/l.

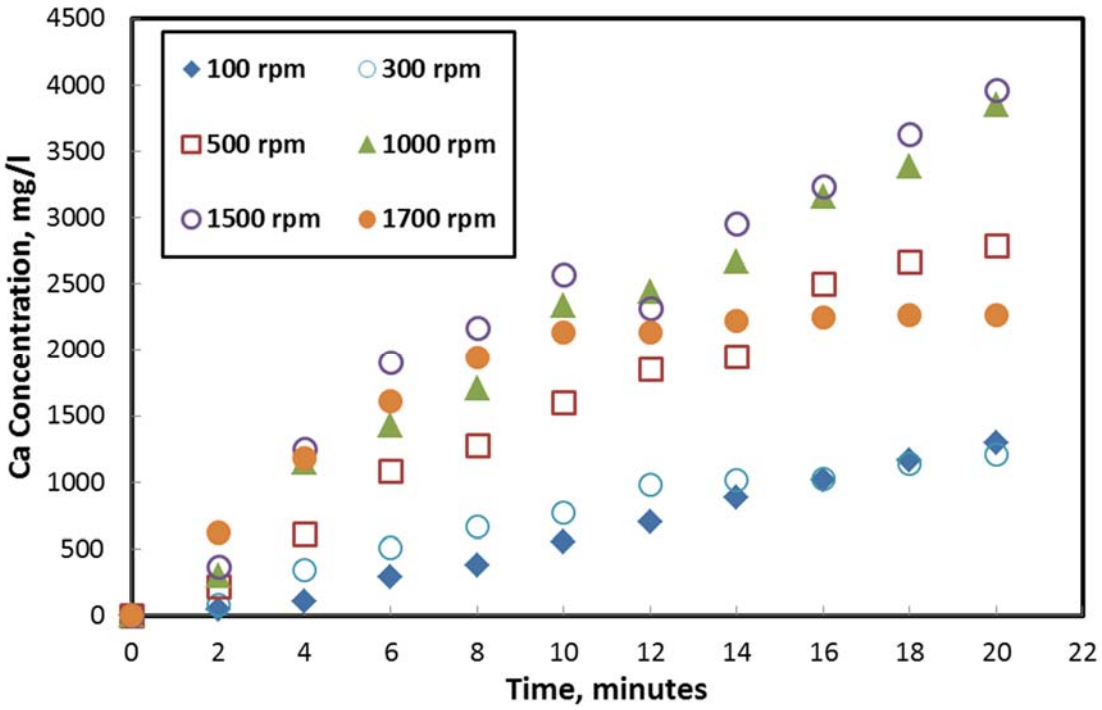

Fig. 3.3- Calcium concentration as a function of time for the reaction of a 10 wt% new organic acid with Indiana limestone at 200°F.

When the temperature was further increased to 250°F, the reaction exhibited a mixed response. **Fig. 3.4** shows that the concentration of calcium increased linearly with time for rotational speeds between 100-500 rev/min. At higher rotational speeds, the calcium concentration increased linearly with time for 10 minutes, then plateaued

afterwards. It is interesting to note that at a rotational speed of 1,700 rev/min, the calcium concentration is lower than that at 1,000 and 1,500 rev/min.

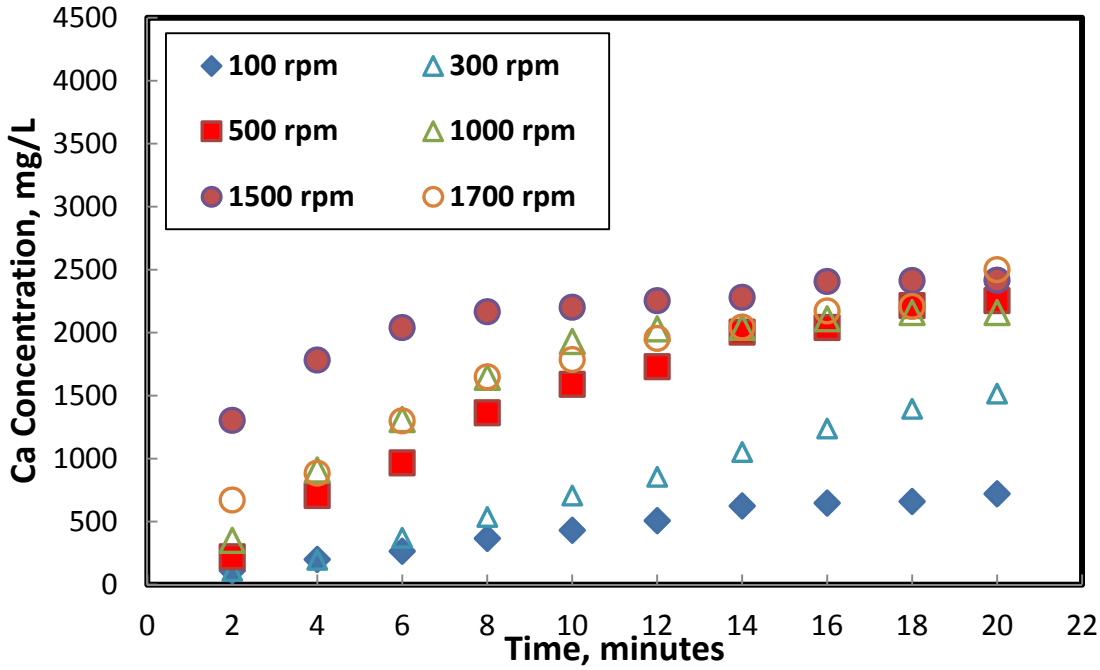

Fig. 3.4- Calcium concentration as a function of time for the reaction of a 10 wt% new organic acid with Indiana limestone at 250°F.

A comparison of **Figs. 3.2 - 3.4** indicates that calcium concentration values at 250°F reached a maximum of 2,500 mg/l, similar to the value reported for 150°F. Subsequently, it can be inferred that by increasing the temperature from 200 to 250°F, the calcium concentration decreased in the range of rotational speeds examined. This decrease was due to the formation of a calcium phosphate precipitate, which is discussed further in the next section.

XRF Analysis of Reacted Disk Surfaces

To determine the nature of the precipitate formed on the disk surfaces, X-Ray Flourescence (XRF) analysis was performed. This analysis indicated the presence of

significant amounts of phosphorus on the disk surfaces, which came from the precipitation of calcium phosphate. **Table 3.3** shows the weight percentage of phosphorus oxide detected as a function of rotational speed for each temperature (150, 200, and 250°F), while **Fig. 3.5** illustrates this data in graphical form.

Table 3.3: Weight % of phosphorus as a function of temperature and RPM.

	P Concentration, %		
RPM	**150°F**	**200°F**	**250°F**
100	1.04	2.74	3.69
500	1.3	2.65	4.47
1000	1.35	3	3
1500	1.09	2.36	1.2

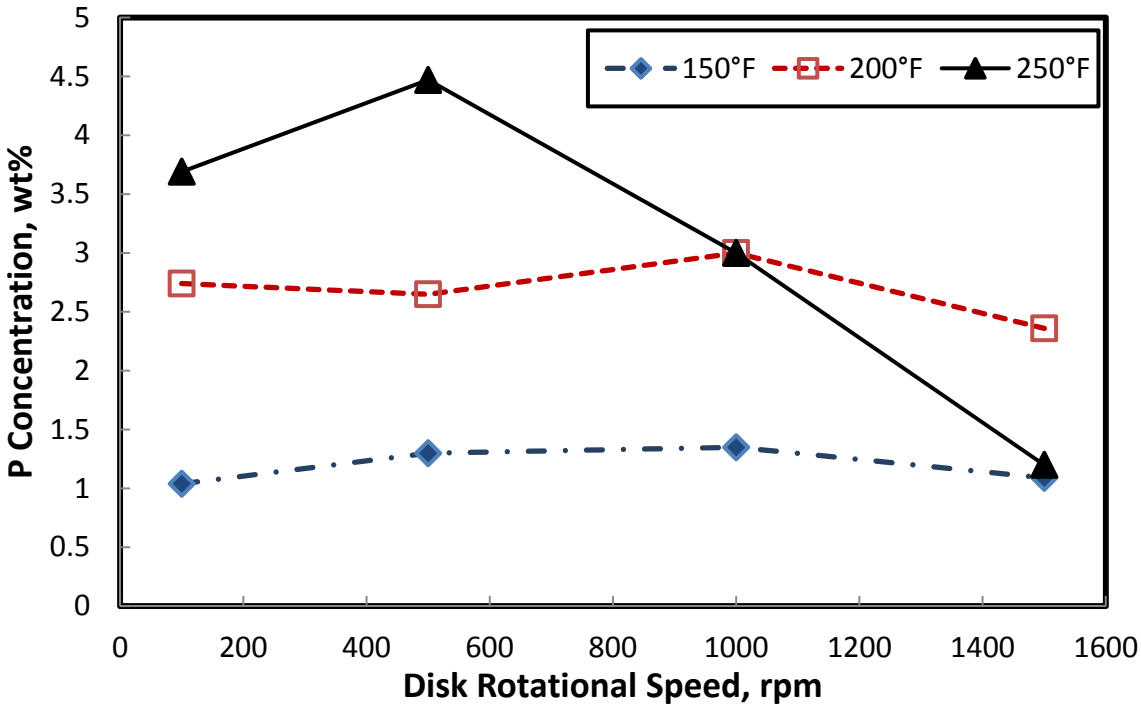

Fig. 3.5- Phosphorus concentration on the surface of the disk as a function of disk rotational speed.

For temperatures of 150°F and 200°F, the amount of phosphorus detected slightly increases from 100 to 1,000 rev/min, but decreases afterwards. At 250°F, the amount of phosphorus detected clearly increases from 100 to 500 rev/min, then decreases rapidly afterwards. Also, it can be seen that for disk rotational speeds between 100 and 500 rev/min, the amount of calcium phosphate precipitate increased with temperature, but afterwards, the correlation became more ambiguous.

Fig. 3.6 shows the amount of phosphorus precipitated as a function of temperature for a disk rotational speed of 500 rev/min. A strong exponential correlation is observed between the temperature and the concentration of phosphorus detected on the surfaces of the core samples. However, for a rotational speed of 1,000 rev/min, the

relationship is less pronounced as the concentration of phosphorus increased from 150 to 200°F, but remained the same for 250°F.

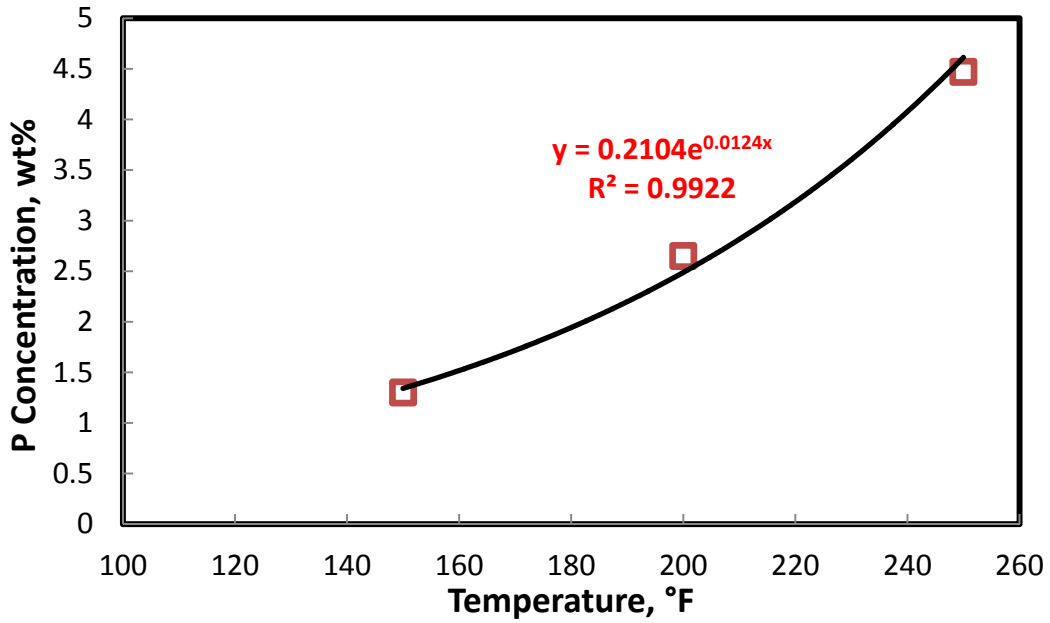

Fig. 3.6- Phosphorus concentration on the surface of the disk as a function of temperature at a disk rotational speed of 500 rpm.

Hot Rolling Oven Analysis of the New Organic Acid

Crushed calcium carbonate was dissolved in a 10 wt% solution of the new organic acid. The resulting mixture was placed in the Teflon liner of a reaction cell. After heating to 300°F for 4 hours, a black precipitate was observed in the solution. To determine the nature of this precipitate, it was filtered from the solution, dried, and analyzed using SEM (Scanning Electron Microscopy). The results are shown below in **Table 3.4**, while the spectrum is labeled as **Fig. 3.7**. Individual peaks relating to different elements are identified. While peaks for calcium, oxygen, and carbon represent

un-dissolved calcium carbonate, it is clear that the calcium phosphate precipitated from the acid during the heating process. This experiment, combined with the results from the XRF studies, affirms that the new organic acid precipitates calcium phosphate at high temperatures (greater than 200°F).

Table 3.4: Results of Scanning Electron Microscopy (SEM).

Elements:	WT%	AT%	K_A	K_F	K_Z	Intensity	P/bkg
C K	59.21	82.31	0.192	1	1.033	0.091	0
P K	5.73	3.09	0.841	1.009	0.938	0.283	1.6
CaK	35.06	14.61	1.037	1	0.945	1.813	8.5

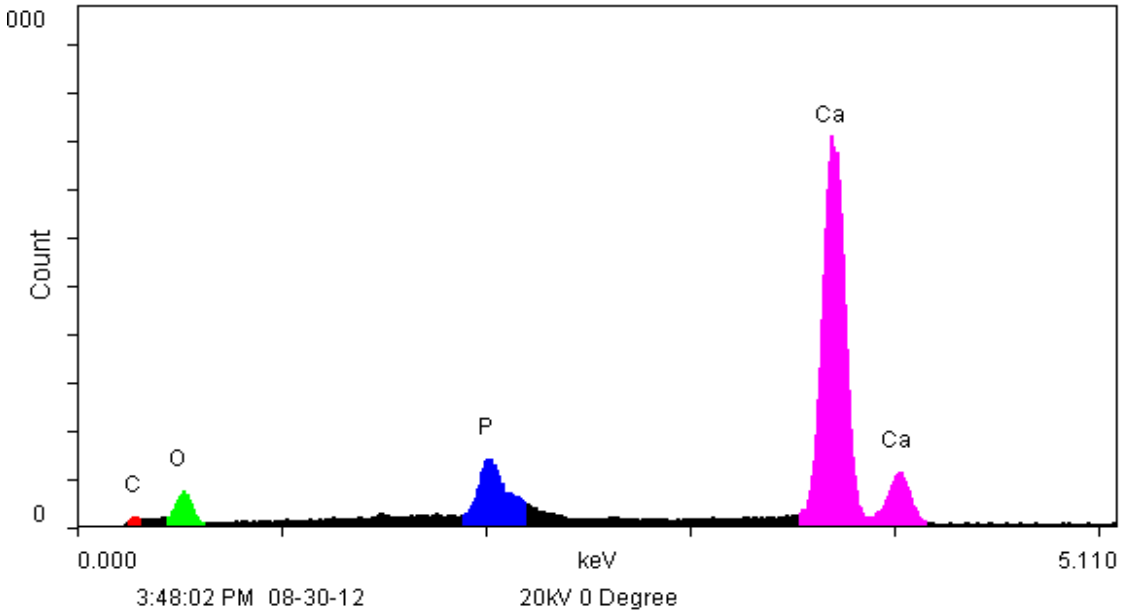

Fig. 3.7- Scanning Electron Microscope (SEM) micrograph for the solids on the disk surface after the reaction with 10 wt% new organic acid (sample A).

Modification of the New Organic Acid to Address the Precipitation Problem

The main source of phosphorus was the presence of phosphoric acid in the synthesis process of the organic acid. A decision was made to substitute the phosphoric

acid by an iron-based catalyst. Three new acid samples (B, C, and D) were collected as a side product of the polyol treatment process. From **Table 2.2**, it is clear that the new acid samples contain minor amounts of phosphorus and hence, reduce the problem of phosphorous precipitation. The reaction of the new acid samples with calcite was evaluated using the rotating disk apparatus at a fixed rotational speed of 1,000 rpm and temperatures of 200 and 250°F**.** The reaction rate of the new acid samples with calcite was compared to that of the original acid sample. The core samples were examined again under the XRF and SEM in order to evaluate the potential for precipitate formation and hence the occurrence of formation damage.

Fig. 3.8 shows the calcium ion concentration in the collected samples as a function of time for the experiments at 200°F. It is clear that the calcium concentration increased with time for each of the four acid samples. Using sample A resulted in a maximum calcium concentration of 4,000 mg/l, while using sample C resulted in a maximum concentration of only 2,500 mg/l.

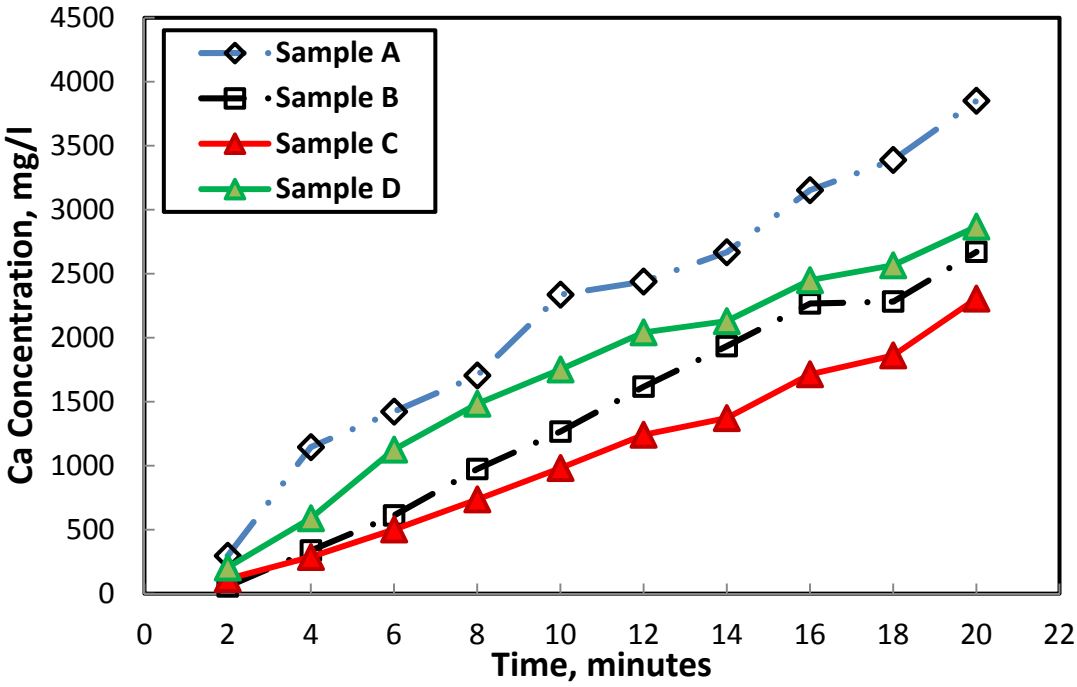

Fig. 3.8- Calcium concentration as a function of time for the reaction of the different new organic acid samples with Indiana limestone at 200°F and 1,000 rpm.

Fig. 3.9 shows the calcium ion concentration in the collected samples as a function of time for the experiment at 250°F. While calcium concentration increased with time for the experiments using sample C, the behavior was different for the experiments using samples A and B. Using sample A, the calcium concentration increased with time reaching a value of 2,200 mg/l at 12 minutes of reaction time, after which it plateaued due to the aforementioned calcium phosphate precipitation. For sample B, the calcium concentration reached a maximum of approximately 2,600 mg/l at 16 minutes, after which the data plateaued. Meanwhile, the use of sample D resulted in a maximum calcium concentration of about 3,000 mg/l, which was higher than the other acid samples.

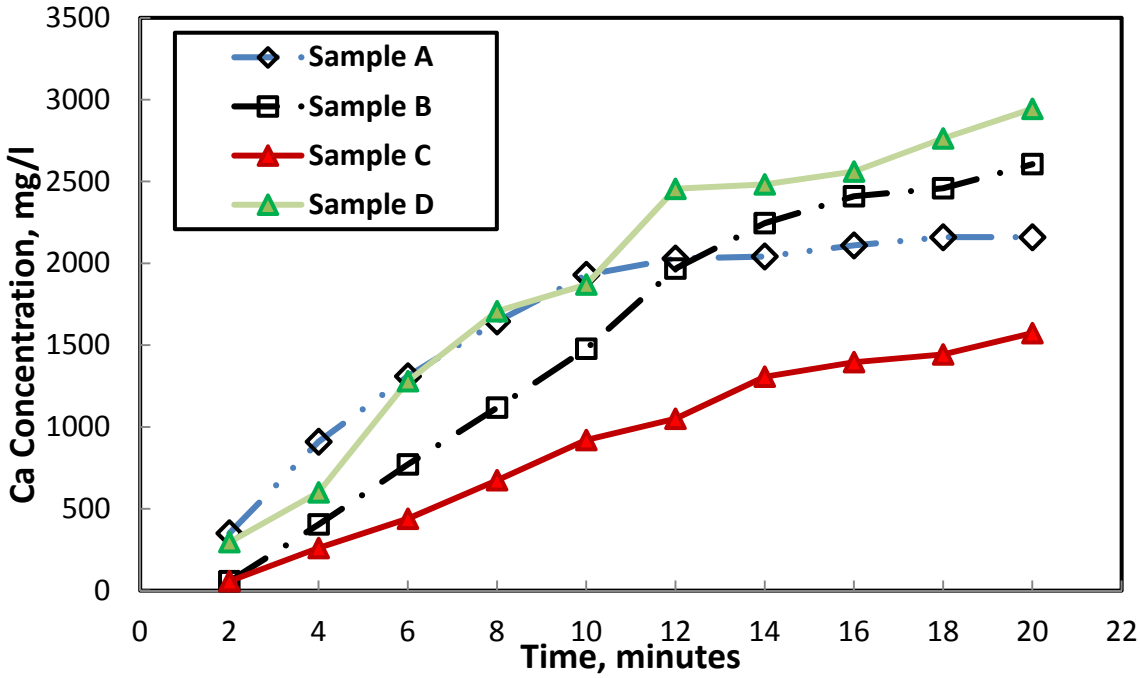

Fig. 3.9- Calcium concentration as a function of time for the reaction of the different new organic acid samples with Indiana limestone at 250°F and 1,000 rpm.

Comparing **Figs. 3.8** and **3.9** leads to two observations. First, sample D resulted in a higher maximum calcium concentration at 250°F than at 200°F. Second, the data for calcium concentration did not plateau after a certain time. Both observations indicate that sample D, unlike A, did not cause a significant amount of precipitation at higher temperatures.

Furthermore, XRF analysis was performed on the core samples used in these experiments. **Fig. 3.10** shows the amount of iron precipitation on each core used in the reactions at 200°F, while **Fig. 3.11** shows the same for the cores used at 250°F.

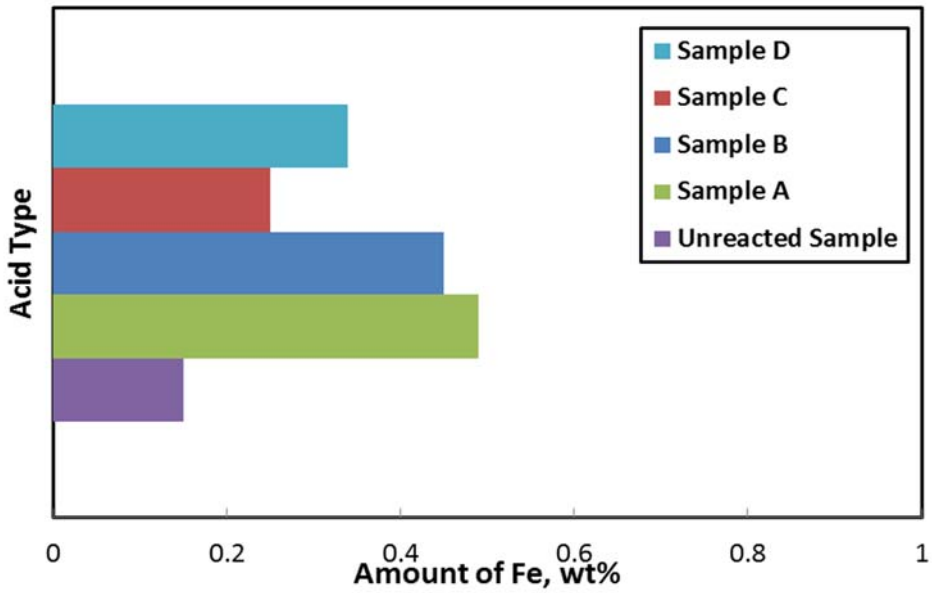

Fig. 3.10- Iron concentration on the disk surface after reaction with 10 wt% new organic acid at 200°F and 1,000 rpm as determined by XRF.

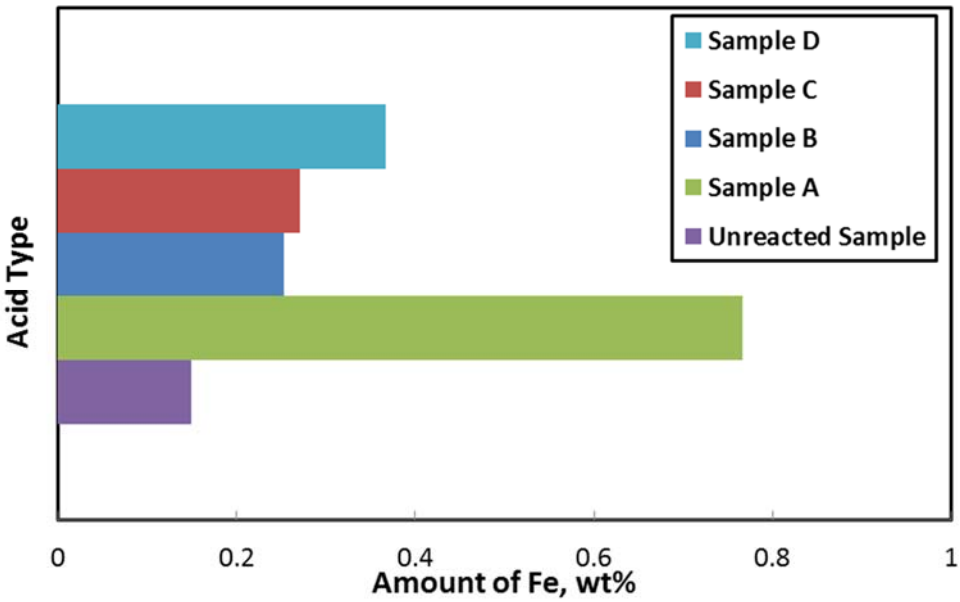

Fig. 3.11- Iron concentration on the disk surface after reaction with 10 wt% new organic acid at 250°F and 1,000 rpm as determined by XRF.

By comparing **Figs. 3.10** and **3.11**, it is clear that the phosphorus-based acid (sample A) had the highest amount of iron precipitation at both temperatures. Also, by increasing the temperature, the amount of precipitation on the cores used with sample A

increased from 0.5 to 0.77 wt%. For sample B, iron precipitation on the cores decreased with the increase in temperature from 0.45 wt% to 0.25 wt%. However, the cores used with sample C exhibited the same amount of iron precipitation (0.27 wt%) at both reaction temperatures. For sample D, iron precipitation on its corresponding cores increased with the increased temperature from 0.339 wt% at 200°F to 0.367 wt% at 250°F. This increase in the amount of iron was not reflected in the reaction rate data as the reaction rates for samples B and D increased with temperature.

Fig. 3.12 shows the effect of temperature on the reaction rates for the three acid samples at a fixed rotational speed of 1,000 rpm. For samples A and C, increasing the reaction temperature from 200 to 250°F resulted in a decrease in the reaction rate. For sample B, however, the temperature increase caused a 20% increase in the reaction rate. Sample D exhibited the highest increase (24%) in reaction rate with the increase in temperature. In the next chapter, this occurrence will come into effect when less volume of sample D is required to achieve breakthrough in 6 in. long Indiana limestone cores than sample B using the coreflood apparatus at 300°F.

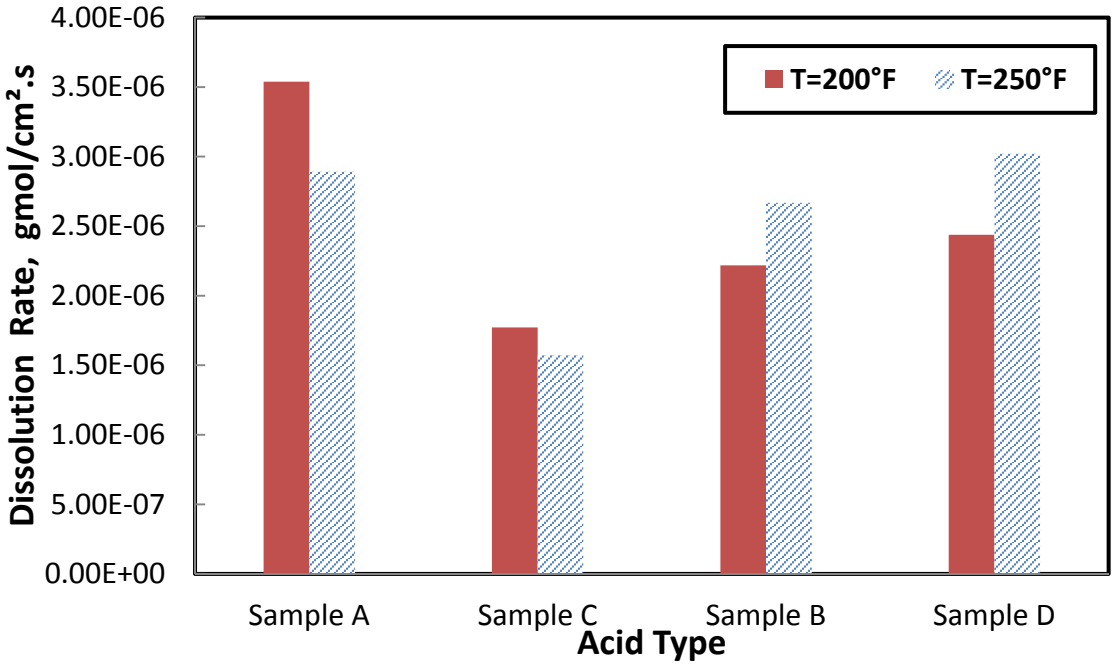

Fig. 3.12 - Effect of temperature on the reaction rates of the three new organic acid samples with Indiana limestone.

Effect of Temperature on the Diffusion Coefficient of the New Organic Acid

Heterogeneous reactions are ones in which two different phases react together. In these systems (e.g. a solid reacting with a fluid), there are two transport processes that greatly affect the reaction rate: reactant fluid to the solid surface and products away from the surface. The overall reaction is composed of three steps: (1) transfer of reactant from the bulk of solution to the solid surface, (2) the surface reaction, and (3) transfer of products from the surface into the bulk of the solution. The overall reaction speed is controlled by the rate of the slowest step, known as the "rate-limiting step".

In order to study the effect of one step on the overall reaction, it is important to eliminate the effect of the other steps. Therefore, surface kinetics can be determined when the mass transport process is faster than the rate of surface reaction. On the other

hand, if the diffusion to the surface is slower than the rate of surface reaction, the main resistance lies in the mass transfer boundary layer, and the reaction is called mass transfer limited. In this case, the rate of dissolution (r_D) can be determined for Newtonian fluids from the flux of the reactant to the surface (J) as shown in **Eq. 3.2** (Levich, 1962; Newmann, 1966; Ellsion, 1969).

$$J = k_m(C_b - C_s) \quad \text{(3.2)}$$

The mass transfer coefficient, k_m, under laminar flow conditions ($Re \leq 3*10^5$ and $Sc > 100$) is defined as follows:

$$k_m = \frac{0.62048(Sc^{-\frac{2}{3}})(\sqrt{v\omega})}{1+0.2980\left(Sc^{-\frac{1}{3}}\right)+0.1451(Sc^{-\frac{2}{3}})} \quad \text{(3.12)}$$

$$Sc = \frac{v}{D_e} \quad \text{(3.13)}$$

$$v = \frac{\mu}{\rho} \quad \text{(3.14)}$$

When mass transfer to the surface is the rate-limiting step, the concentration of reactant at the surface (C_s) can be ignored with respect to the initial concentration (C_b). Rearranging the variables in **Eq. 3.2**, **Eq. 3.14** can be obtained:

$$k_m = \frac{J}{C_b} \quad \text{(3.15)}$$

In the mass transfer regime, the calcite dissolution rate is equal to the mass flux of the new organic acid, *J*, and based on **Eq. 3.15**, it will have a linear relationship with the square root of the disk rotational speed.

$$J = \left\{ \frac{0.62048(Sc^{-\frac{2}{3}})(\sqrt{\nu})}{1+0.2980\left(Sc^{-\frac{1}{3}}\right)+0.1451(Sc^{-\frac{2}{3}})} * C_b \right\} * \omega^{0.5} \quad \text{.....(3.16)}$$

From the slope of the straight lines in **Fig. 3.1**, the Schmidt number can be calculated; hence, the diffusion coefficient of the new organic acid can be determined using **Eq. 3.11**. The calculated values for the diffusion coefficient are shown below in **Table 3.5** and plotted in **Fig. 3.11**. Due to the precipitation of calcium phosphate documented above, the diffusion coefficient of the acid at 250°F was lower than its counterpart at 200°F.

Table 3.5: Effect of temperature on the diffusion coefficient of the new organic acid at 10 wt% and 1,000 psi.

T, °F	T, K	1/T, K^{-1}	D, cm^2/s
150	338.5556	0.002954	2.07366E-05
200	366.3333	0.00273	3.17303E-05
250	394.1111	0.002537	1.83568E-05

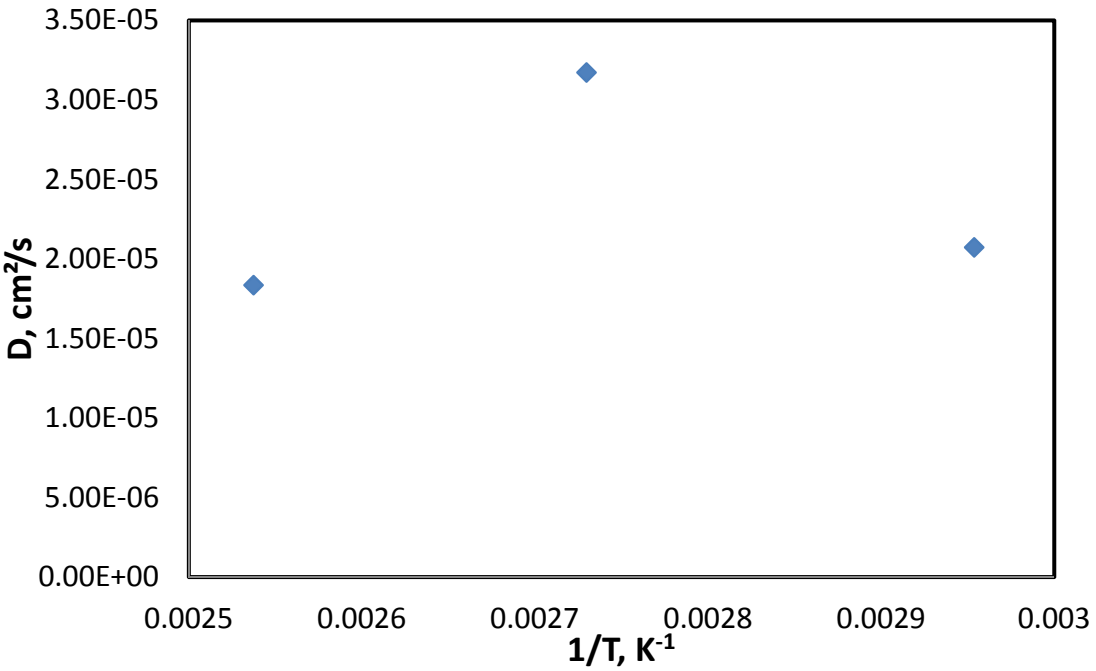

Fig. 3.13- Diffusion coefficient of 10 wt% sample A of the new organic acid as a function of temperature.

The temperature dependence of diffusion coefficients is usually quantified using the Arrhenius equation:

$$D = D_0 \exp(-\frac{E_a}{RT}) \quad \text{.....(3.17)}$$

From **Fig. 3.13**, it is evident that the effect of temperature on the diffusion coefficient of the new organic acid does not follow Arrhenius law after 200°F. However, it is proposed that the diffusion coefficient at a temperature between 150 and 200°F be investigated to see if an Arrhenius relationship can be established for this temperature range.

Compared to HCl and other organic acids (e.g. acetic, citric, and formic acid), the new organic acid (sample A) has a lower diffusion coefficient at 93°C (200°F) than the aforementioned acids do at 25°C. For example, the diffusion coefficient of 0.25M new organic acid is 3.17E-5 cm^2/s, while the diffusion coefficients of 0.5M HCl, 0.5M acetic acid and 0.5M formic acid are 3.6E-5 cm^2/s, 1.1E-5 cm^2/s, and 3.0E-5 cm^2/s, respectively (Buijse et al. 2004; Kung, 1998).

Conclusions

Four samples of a new organic acid were tested in this study. One sample was made with a phosphorus-based catalyst, where the other three samples were made with an iron-based catalyst. For the phosphorus-based sample, the following conclusions can be made:

1. At low temperatures (150°F), the reaction was controlled by surface reaction kinetics at disk rotational speeds higher than 500 rpm.
2. At high temperatures (200 and 250°F), the reaction was controlled by the rate of mass transfer of the acid to the disk surface.
3. At 250°F, the reaction rate of the acid with calcite decreased, in comparison to 200°F, due to the formation of a calcium phosphate.
4. Due to the aforementioned precipitation, an Arrhenius relationship between temperature and the diffusion coefficient could not be established above 200°F.

For the iron-based samples, the following conclusions can be made:

1. At 200°F, the reaction rates of samples B, C, and D with calcite were less than that of the sample A.

2. At 250°F, the reaction rates of samples B and D increased from their values at 200°F, while that of sample C decreased slightly.

CHAPTER IV

COREFLOOD EVALUATION OF THE NEW ORGANIC ACID

Introduction

The main objective of matrix stimulation is to create highly conductive permeable channels, known as wormholes, which allow the flow of oil and gas. The transport of the reacting component is a function of its diffusivity and flow rate, while the surface reaction is affected significantly by the surface kinetics. Several studies, including Fredd and Fogler (1999), have reported that there is an optimum flow rate that results in a minimum volume of injection fluid required to form these wormholes until breakthrough. Often, the injection volume of the fluid is given as a pore volume number which represents the ratio of the total volume of the injected fluid to the pore volume in a rock sample. The injection rate that corresponds to the minimum pore volume is expressed in terms of the Damköhler number, which is defined as follows in **Eq. 4.1** (Fredd and Fogler 1998b):

$$Da = \frac{\pi dlk}{Q} \quad \text{.....(4.1)}$$

where:

$k = k_m = 1.86 D_e^{\frac{2}{3}} (\frac{u}{dl})^{1/3}$, if reaction is mass-transfer limited

$k = k_{sr}$, if reaction is surface reaction limited

In the previous chapter, the reactions of four samples of the new organic acid were examined, and the effects of disk rotational speed and temperature were investigated. In this part of the investigation, 10 wt% solutions of three samples of the

new organic acid were used to stimulate Indiana limestone cores. The objectives of this part of the study are to: (1) determine the potential for formation damage when the new organic acid was used to stimulate limestone cores at high temperatures, (2) determine the acid sample that will take the least amount of fluid to create wormholes and, (3) determine the optimum injection rate of the chosen sample at 300°F.

Experimental Studies

Materials

Core samples from blocks of Indiana limestone were cut into cylinders 6 in. long and 1.5 in. in diameter. Samples were saturated in water and the weight of the samples was measured before (dry) and after saturation. The average porosity was 13.4 vol%.

Acid Preparation

The new organic acid was obtained at an initial concentration of 50 wt%. For the experimental procedure, the acid was diluted to a concentration of 10 wt%. To do so, de-ionized water was obtained from a water purification system that has a resistivity of 18.2 MΩ.cm. Also, 0.1 vol% corrosion inhibitor (proprietary alkoxylated fatty amine salts, alkoxylated organic acid, Thiourea, N, N'-dibutyl) was added to prepare the acid.

Coreflood Apparatus

Coreflood tests were run at different flow rates using the same acid preparation method described above. In order to maintain the acidizing process at a constant temperature of 205°F, two temperature controllers were used. The temperature of the preheated fluids coming from the accumulators is controlled by a compact bench top CSC32 series, which has a 4-digit display, 0.1° resolution with an accuracy of ±0.25%

full scale ±1°C. It uses a type K thermocouple and two outputs (5 A 120 Vac SSR). Before running the coreflood test, the cores were first saturated with deionized water and their pore volumes were calculated. Computer tomographic (CT) scans were performed before and after the treatment to determine the propagation of the wormhole. Using LabView® software, the pressure drop across the core during the treatment was monitored and the core permeability was determined before and after the treatment.

Results and Discussion

Sample A Coreflood at 205°F

An Indiana limestone core with an initial permeability of 1.1 md and porosity of 12% was examined in the core flood experiment that was run using a 10 wt% solution of the new organic acid at a temperature of 205°F. At an injection rate of 2 cm^3/min, it was determined that 6.6 PV had to be injected in order to achieve acid breakthrough, resulting in a final core permeability of 29.5 md. The results for this experiment are shown below in **Fig. 4.1**.

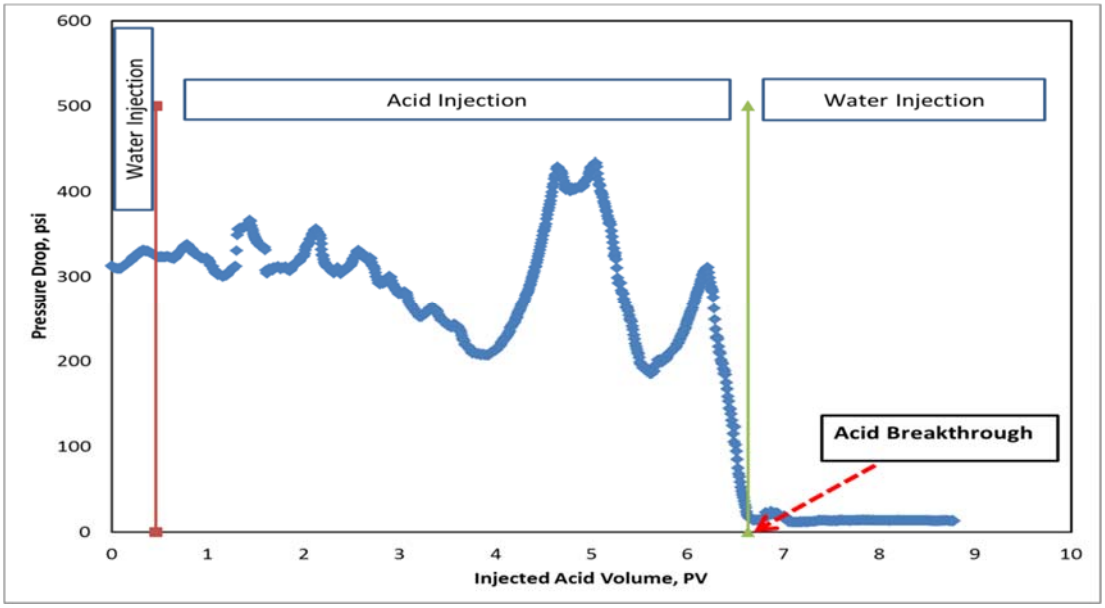

Fig. 4.1- Pressure drop across the core during injection of 10 wt% new organic acid (sample A) at an injection rate of 2.0 cm^3/min.

During the water injection step, the pressure drop across the core was stabilized at a value of 315 psi. After the acid was injected into the core and it started to react with the rock, a pressure cycle of decease and increase was noticed with a general decrease in the pressure drop across the core as a result of the dissolution of calcite and the creation of wormholes. After injection of around 3.6 PV of acid, the pressure drop increased to a value of 430 psi and started to decrease again. This increase in the pressure drop across the core was noticed again after injection of 6 pore volumes of 10 wt% of the original new organic acid. Afterwards, the pressure drop across the core decreased rapidly until the acid broke through the core and the final pressure drop was stabilized at a value of 15 psi. While no face dissolution occurred, wormholes were formed in the core and a CT scan was performed to determine the extent of penetration of these wormholes. As

shown below in **Fig. 4.2**, wormhole size decreased as the acid travelled further inside the core.

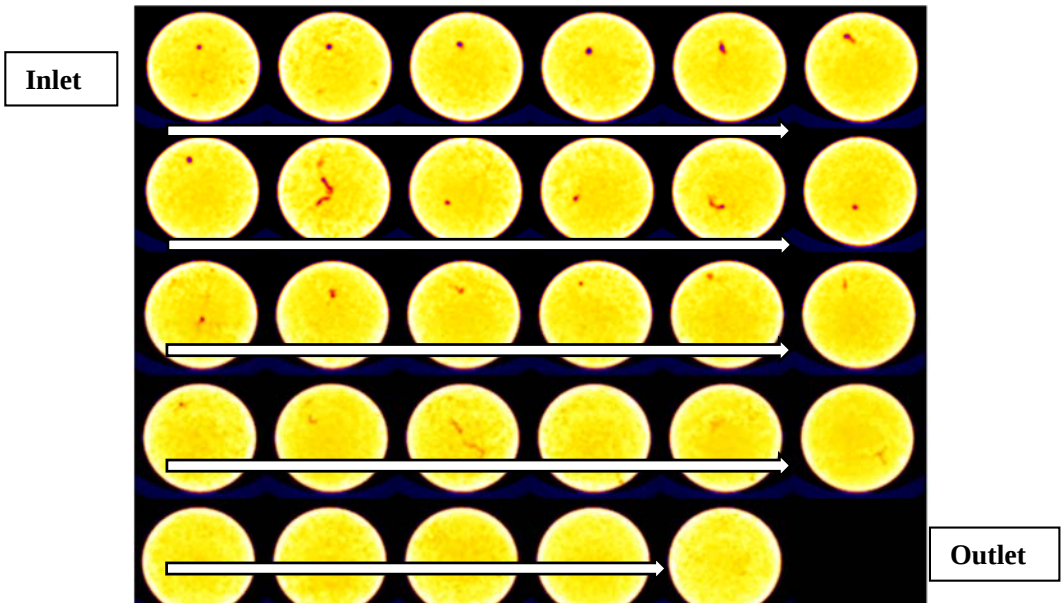

Fig. 4.2: Computer Tomographic (CT) image of the core after injection of acid at injection rate of 2.0 cm^3/min and at 205°F.

Coreflood Tests at 300°F (Samples A, B, and D)

Sample A

Since the aim of this investigation is to evaluate the performance of the new organic acid for HPHT applications, a second experiment was conducted using sample A at 300°F. This experiment failed as the acid reacted with the formation to form a calcium phosphate precipitate on the core face and inside it. This is clearly shown in **Fig. 4.3**, where wormholes appear on the inlet face of the core, but not on the outlet.

Fig. 4.3- Photographs of an Indiana limestone core used with sample A after treatment at 300°F (left) inlet face and (right) outlet face.

In order to ascertain the nature of the precipitate, scanning electron microscopy (SEM) analysis was performed on the precipitate observed on the face of the core and inside it. Below, **Fig. 4.4** shows the labeled spectrum for the results and **Table 4.1** shows the results in numerical form. The results indicate that phosphorus was detected, proving that calcium phosphate precipitation occurred.

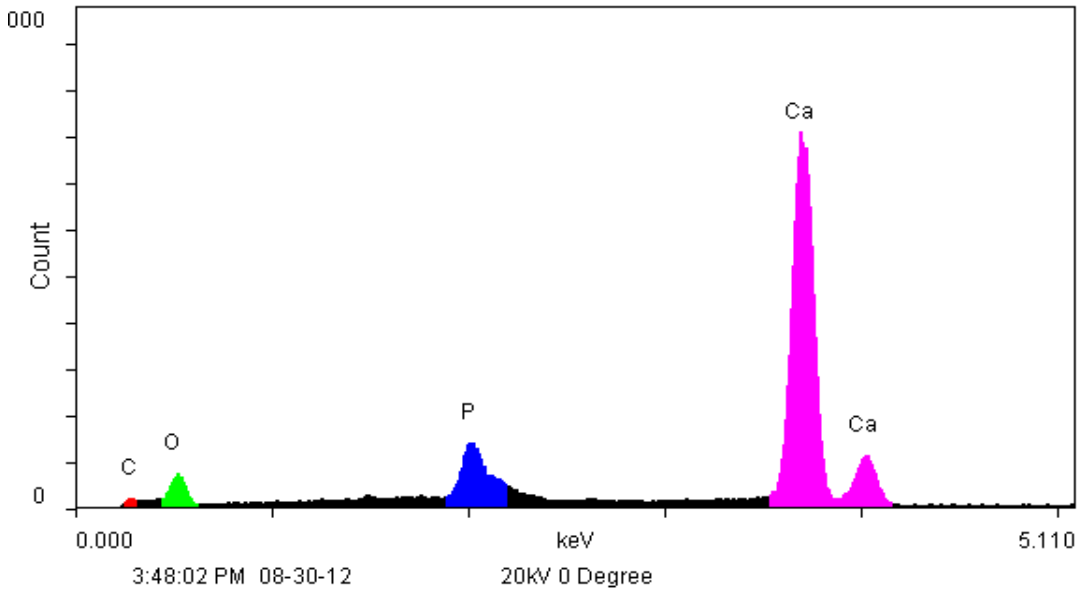

Fig. 4.4- Scanning Electron Microscope (SEM) micrograph for the solids on the core surface after reaction with 10 wt% new organic acid (Sample A).

Table 4.1: Results of Scanning Electron Microscopy (SEM) for the solids on the core surface after reaction with 10 wt% sample A.

Elements:	WT%
C K	59.21
P K	5.73
CaK	35.06

Sample B

For this coreflood experiment, the pressure drop across the core was plotted using LabView software. Samples of the coreflood effluent were analyzed for calcium and iron concentrations. **Fig. 4.5** shows the pressure drop across the core during the injection of the 10 wt% organic acid at an injection rate of 2 cm^3/min and 300°F. During the initial period of water injection, the pressure drop decreased slightly to about 160 psi. Immediately after acid injection was begun, the pressure drop increased slightly due to the viscosity of the acid. As the calcite dissolved and reacted with the organic acid, the calcium concentration of the acid effluent started to increase. At the same time the calcium was reacting with the organic acid, wormholes started to form and penetrate the core. This formation of wormholes caused the pressure drop to decrease again. The increase and subsequent decrease in pressure drop depends mainly on the extent of dissolution in the length of the core.

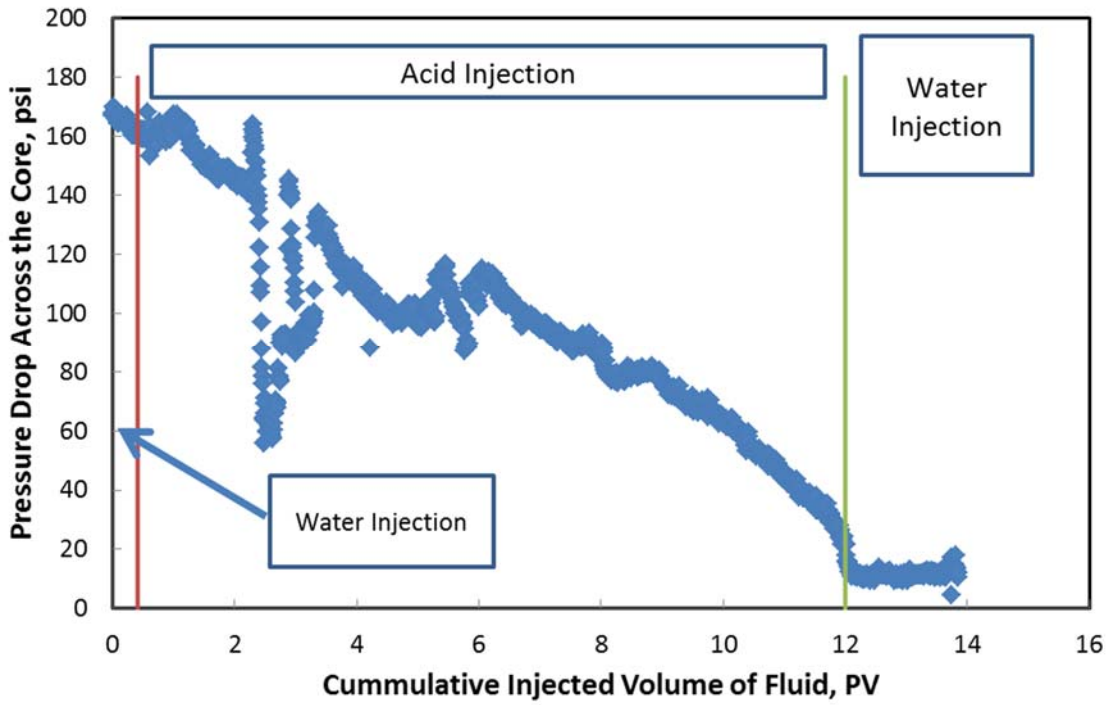

Fig. 4.5- Pressure drop across the core during injection of 10 wt% new organic acid (Sample B) at an injection rate of 2.0 cm³/min and 300°F.

Fig. 4.6 shows the concentration in the core effluent samples for the experiment shown in **Fig. 4.5.** The total calcium concentration reached a maximum value of 8,741 mg/l. Also, **Fig. 4.6** shows the iron concentration in the core effluent samples for the same experiment and indicates that it reached a maximum value of 313 mg/l.

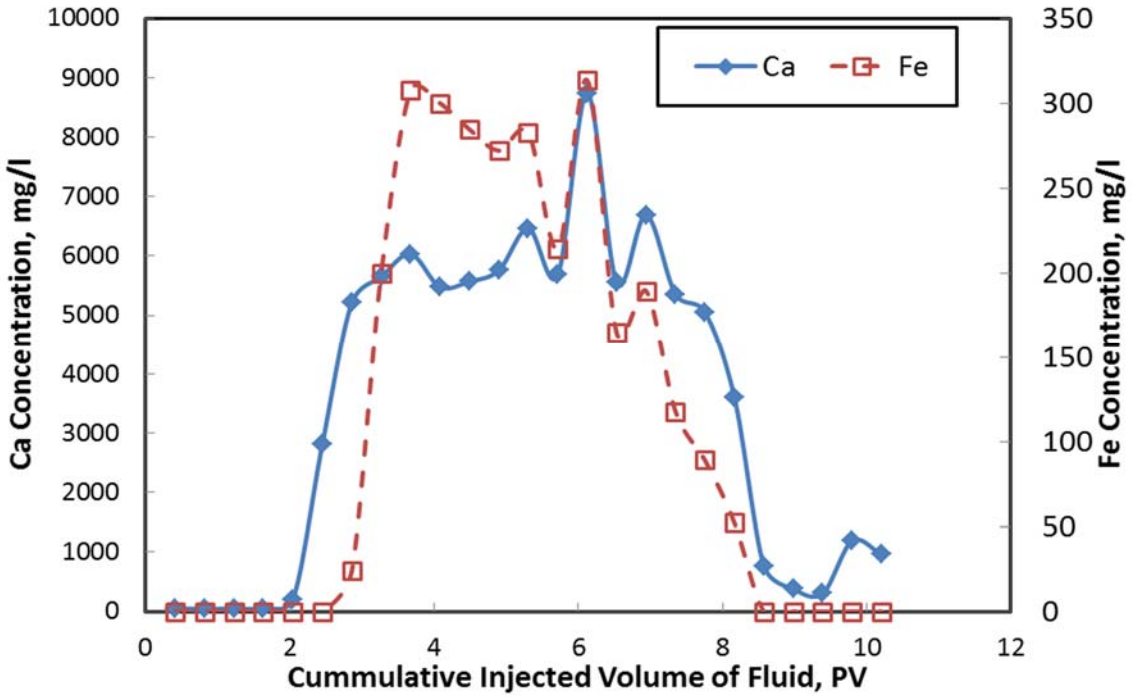

Fig. 4.6- Calcium and iron concentrations in the core effluent samples for the new organic acid (Sample B) at an injection rate of 2.0 cm³/min and 300°F.

Sample D

A second coreflood experiment was conducted using the same procedure described above with sample D of the new organic acid. **Fig. 4.7** shows the pressure drop across the core during the injection of the 10 wt% solution of sample D at an injection rate of 2 cm^3/min and 300°F. During the initial period of water injection, the pressure drop decreased slightly. Immediately after acid injection began, the pressure drop increased slightly due to the viscosity of the acid. As the calcite dissolved and reacted with the organic acid, the calcium concentration of the acid effluent started to increase. At the same time the calcium was reacting with the organic acid, wormholes started to form and penetrate the core. This formation of wormholes caused the pressure

drop to decrease again. The increase and subsequent decrease in pressure drop depends mainly on the extent of dissolution in the length of the core.

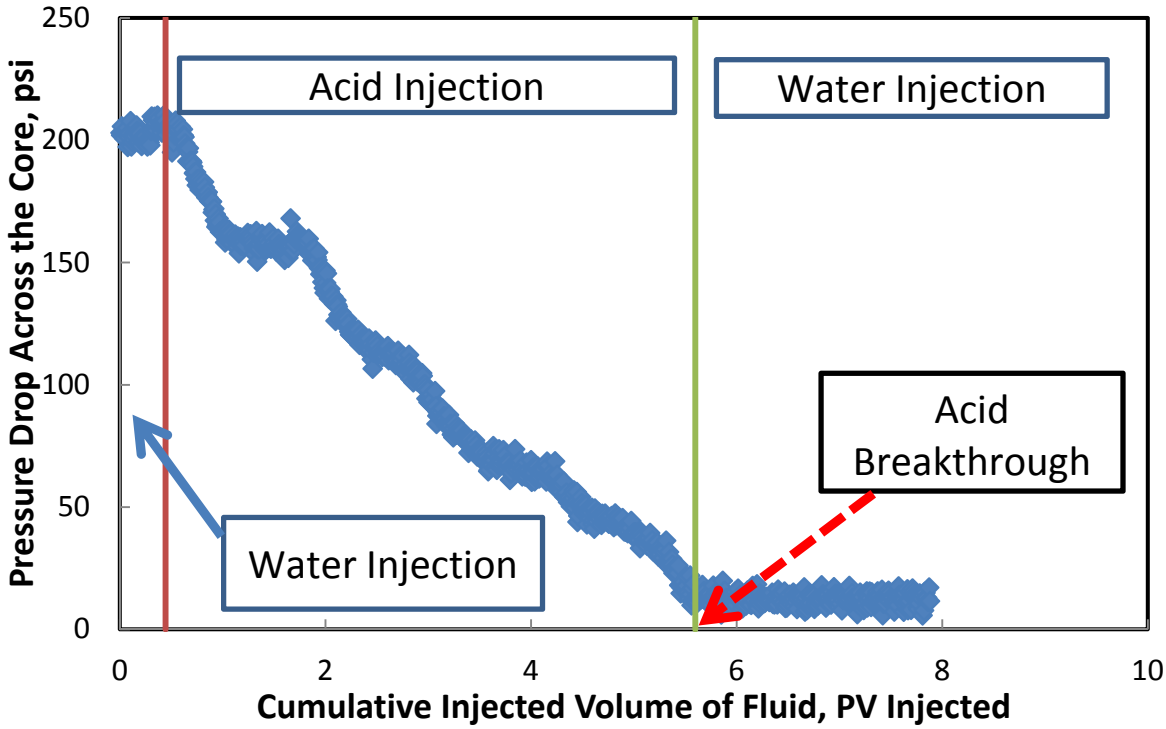

Figure 4.7- Pressure drop across the core during injection of 10 wt% new organic acid (Sample D) at an injection rate of 2.0 cm³/min and 300°F.

Fig. 4.8 shows the concentration in the core effluent samples for the experiment shown in **Fig. 4.7.** The total calcium concentration reached a maximum value of 6,100 mg/l. Also, **Fig. 4.8** shows the iron concentration in the core effluent samples for the same experiment and indicates that it reached a maximum value of 87 mg/l.

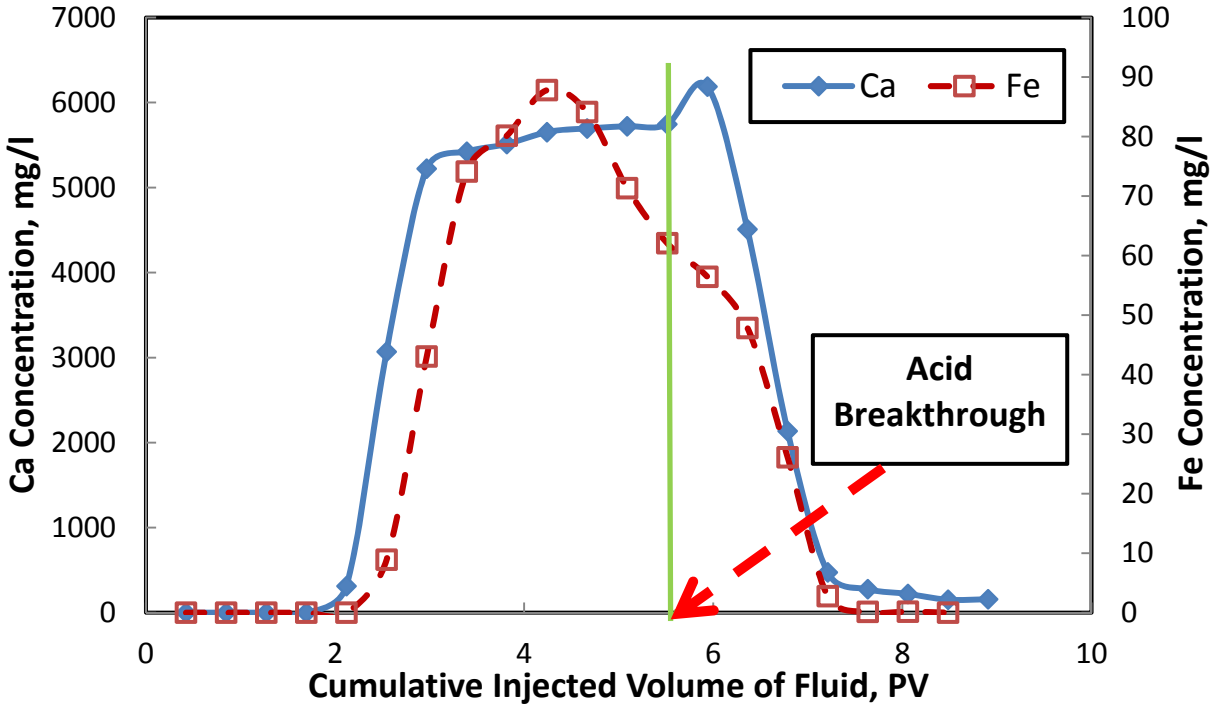

Fig. 4.8- Calcium and iron concentration in the core effluent samples for the new organic acid (Sample D) at an injection rate of 2.0 cm³/min and 300°F.

In comparing the coreflood experiments for samples B and D, it is observed that the maximum calcium and iron concentrations obtained using sample B were higher than sample D. This indicates that the dissolving power of sample B is higher than that of D. However, the lower iron concentration in sample D is a direct result of the lower iron (II) sulfate content used in the synthesis of the this sample. Based on these results, the decision was made to use sample D for the investigation of the optimum injection rate of the new organic acid.

The optimum injection rate for different stimulation fluids has been determined by many investigators. The importance of identifying the optimum injection rate is to achieve the maximum penetration of the stimulation fluid through the treated zone. The

volume of the stimulation fluid required to create deep, uniform wormholes is minimum at the optimum injection rate and therefore, it is necessary to determine the optimum injection rate for the new organic acid. To that effect, six more experiments were conducted by varying the fluid injection rate.

Figs. 4.9-4.14 show the pressure drop across the core during the injection of the 10 wt% solution of sample D at 300°F and injection rates of 0.5, 0.75, 1, 3, 5, and 10 cm^3/min. All of the graphs followed the pattern discussed here. During the initial period of water injection, the pressure drop remained constant. After acid injection began, the pressure drop increased slightly due to the viscosity of the acid. As the calcite dissolved and reacted with the organic acid, the calcium concentration of the acid effluent started to increase. At the same time the calcium was reacting with the organic acid, wormholes started to form and penetrate the core. This formation of wormholes caused the pressure drop to decrease again. The increase and subsequent decrease in pressure drop depends mainly on the extent of the dissolution in the length of the core.

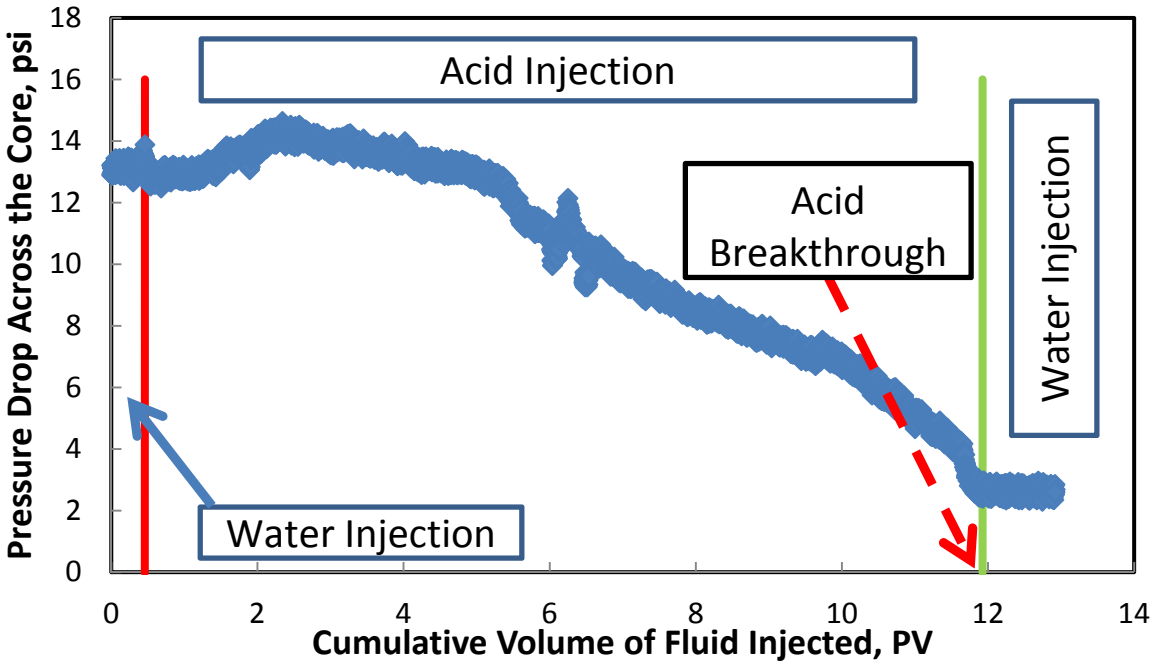

Figure 4.9- Pressure drop across the core during the injection of 10 wt% new organic acid (sample D) at an injection rate of 0.5 cm³/min and 300°F.

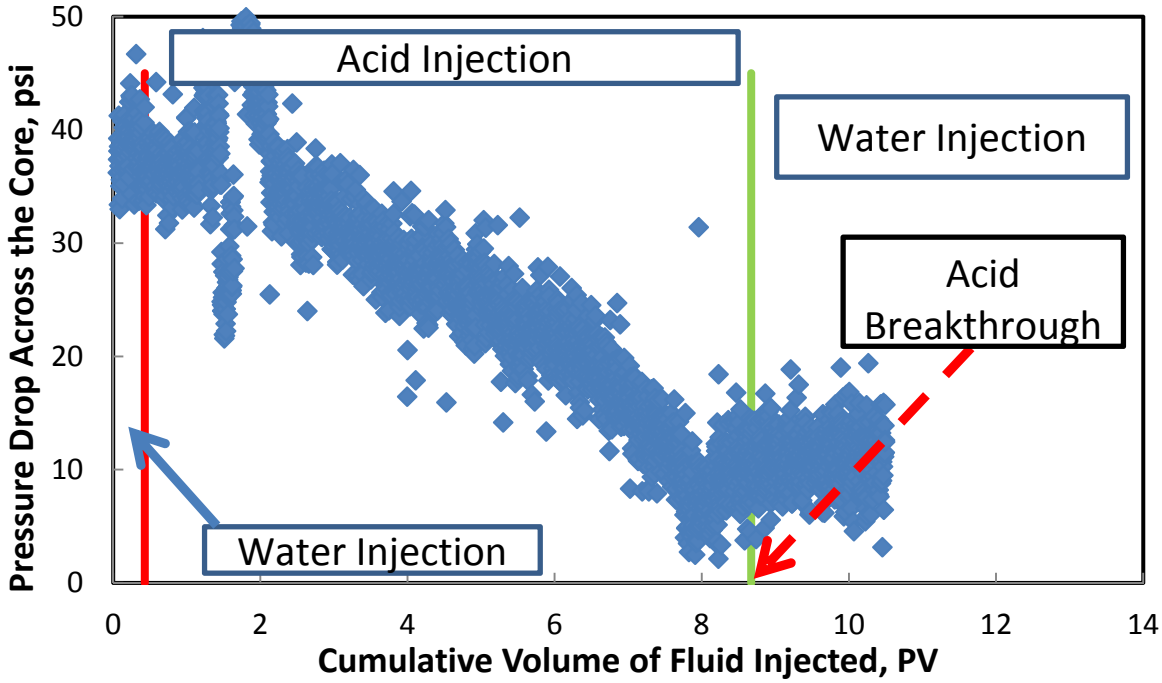

Figure 4.10- Pressure drop across the core during the injection of 10 wt% new organic acid (sample D) at an injection rate of 0.75 cm³/min and 300°F.

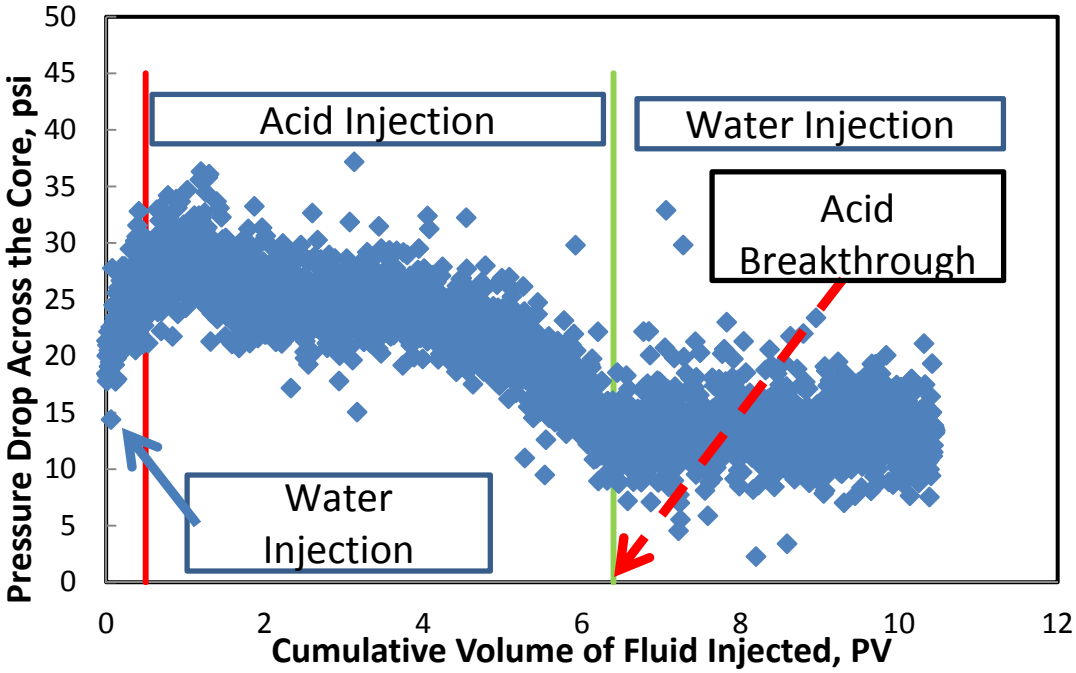

Figure 4.11- Pressure drop across the core during the injection of 10 wt% new organic acid (sample D) at an injection rate of 1.0 cm³/min and 300°F.

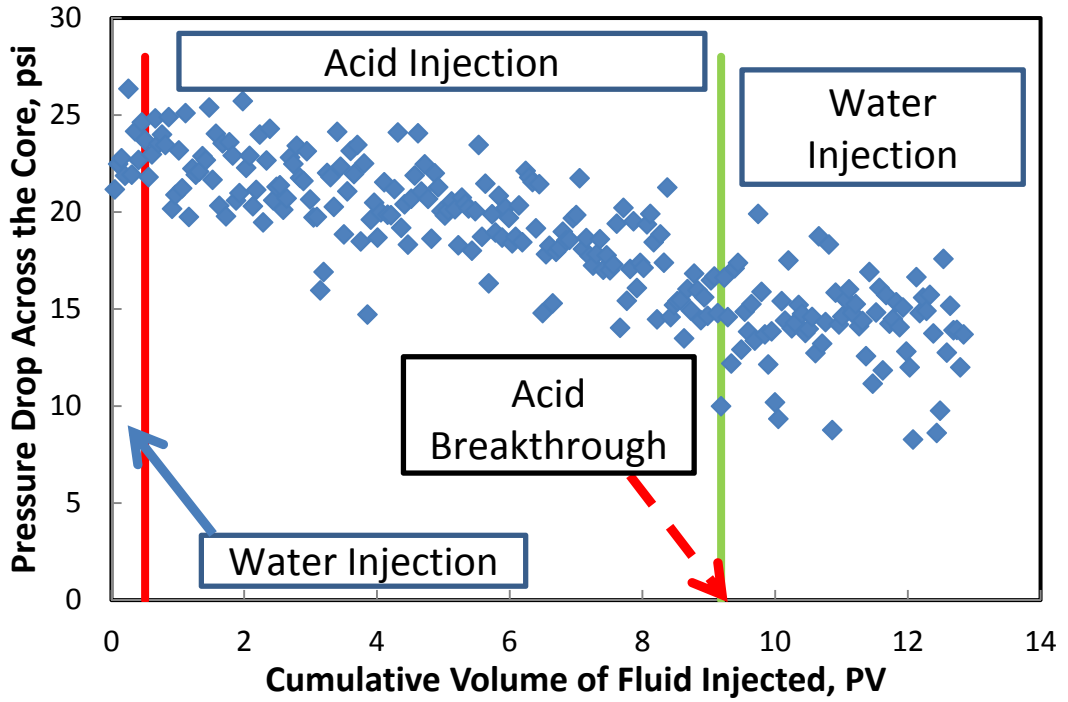

Figure 4.12- Pressure drop across the core during the injection of 10 wt% new organic acid (Sample D) at an injection rate of 3.0 cm³/min and 300°F.

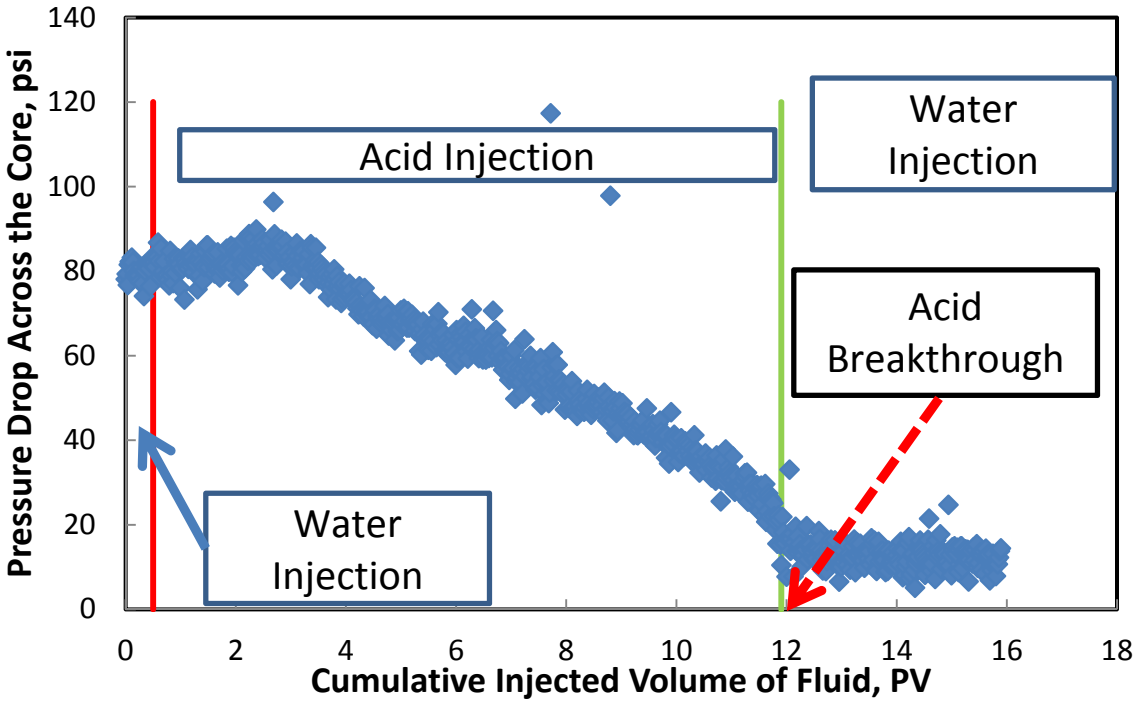

Figure 4.13- Pressure drop across the core during the injection of 10 wt% new organic acid (Sample D) at an injection rate of 5.0 cm³/min and 300°F.

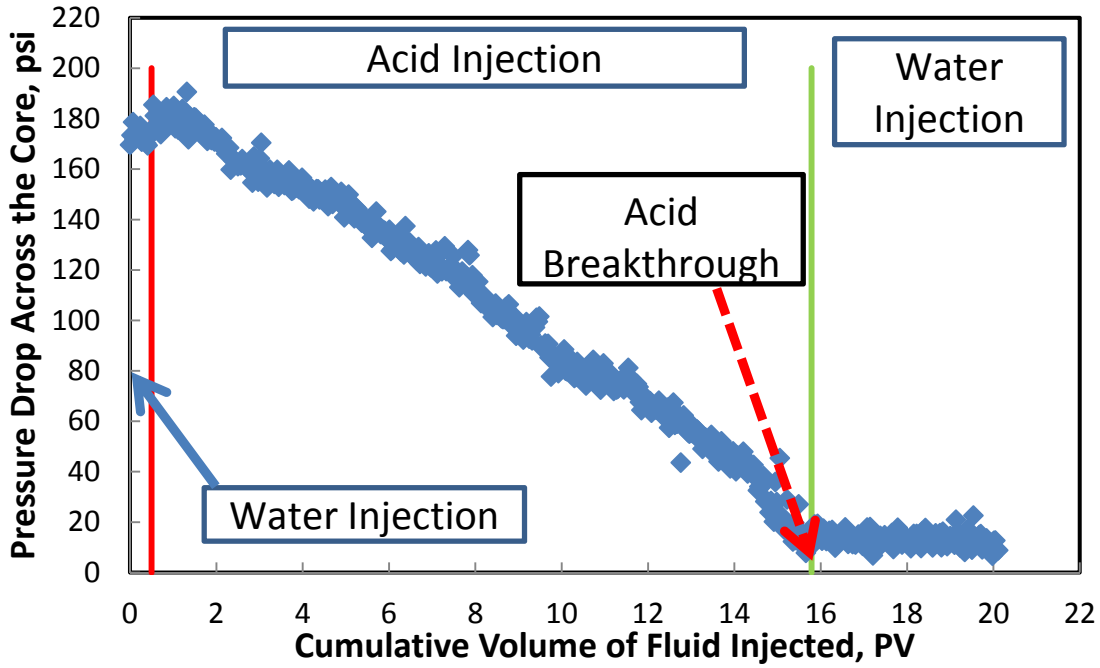

Figure 4.14- Pressure drop across the core during the injection of 10 wt% new organic acid (Sample D) at an injection rate of 10.0 cm³/min and 300°F.

Table 4.2 gives the data for the coreflood experiments that were run at 300°F. The PV at breakthrough (PV_{bt}) was 5.59 at the optimum injection rate, and at injection rates below the optimum, for example at 1 cm^3/min, the PV_{bt} was 6.40 PV. At injection rates greater than the optimum, for example at 5 cm^3/min, the PV_{bt} was 11.91 PV.

Table 4.2: Coreflood data for optimum injection rate investigation.

Exp. #	Q, cm^3/min	$K_{initial}$, md	∅, vol%	PV_{bt}
1	0.5	5.2	12.95	11.93
2	0.75	5.3	12.34	8.61
3	1.00	10.4	14.20	6.40
4	2.00	5.5	13.20	5.59
5	3.00	10.1	14.18	9.34
6	5.00	10.0	13.10	11.91
7	10.0	14.0	13.50	15.87

Fig. 4.15 shows the optimum injection rate for 10 wt% new organic acid using Indiana limestone cores (2 cm^3/min). The relationship between injection rate and PV_{bt} for the new organic acid was not the same as that for HCl. At low injection rates, HCl caused face dissolution and required high volumes to create wormholes. When injected at low rates (0.5 or 1 cm^3/min), the new organic acid did not require as many PV as HCl did because of its low reaction rate (discussed in Chapter III of this study). In the case of the new organic acid, low injection rates allowed more time for the reaction and dissolved larger amounts of calcite than at high injection rates. A similar trend was obtained and for the 10 wt% Na_4EDTA solution reported by Huang et al. (2003) and the

20 wt% GLDA at 180°F in Mahmoud et al. (2011). Fig. 4.16 shows this comparison in graphical form.

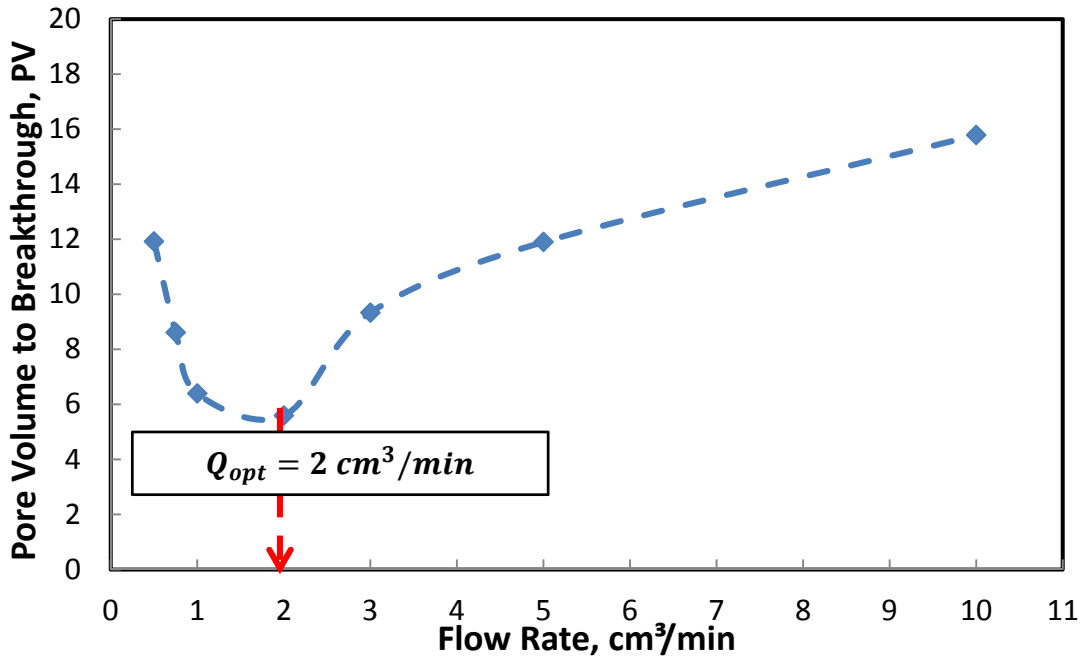

Fig. 4.15- Pore volumes to breakthrough for 10 wt% new organic acid (sample D) at 300°F.

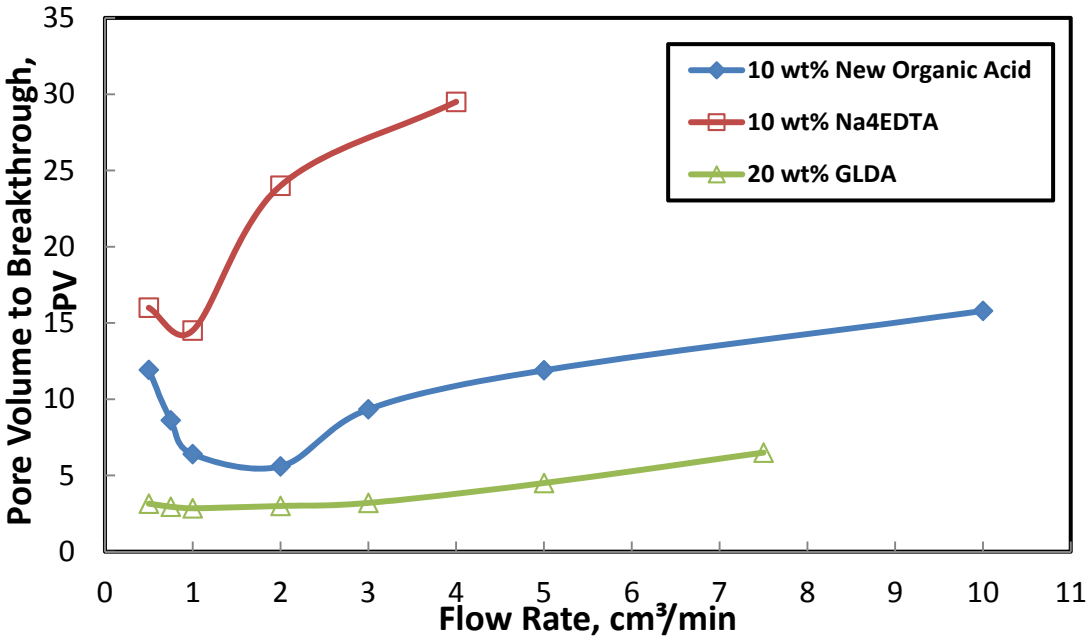

Fig. 4.16- Comparison of 10 wt% new organic acid, 10 wt% Na_4EDTA, and 20 wt% GLDA.

Fig. 4.17 shows the calcium concentration in the core effluent samples for all the experiments. The reaction rate of this acid is slower than HCl; therefore, injecting the organic acid at low injection rates allowed more time for the reaction. Therefore, less volume of the fluid was required to create wormholes.

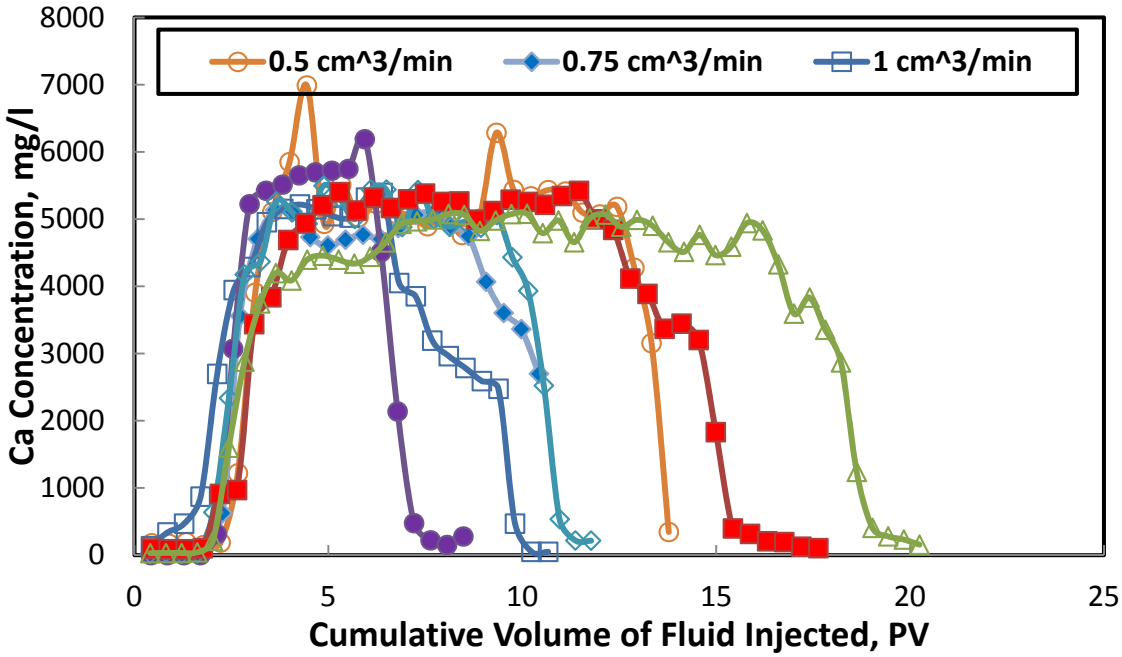

Fig. 4.17- Calcium concentration in the core effluent samples for the new organic acid (sample D) for all injection rates.

At injection rates below the optimum, the PV required to break through the core was higher than that required to do so at the optimum rate. There was one dominant wormhole that penetrated through the core. The other wormholes did not penetrate through the core, and they consumed a greater volume of acid. At the optimum injection rate, there was one dominant wormhole and thus, the PV required to create this wormhole was the smallest. As for higher injection rates, the PV required to create

wormholes was greater than that required to do so at the optimum rate. At higher injection rates, the increase in the PV was greater as compared to the increase in PV for injection rates below the optimum rate. This is due to the lack of sufficient time for the organic acid to react with the rock, which meant that the acid was able to dissolve small amounts of the rock. To form a dominant wormhole, a greater volume of the organic acid was required to compensate for the decrease in contact time.

Fig. 4.18 shows the wormholes created at the core inlet faces for the cores used with 10 wt% new organic acid.

Fig. 4.18- Wormholes at the core inlet surfaces in order of increasing injection rate of 10 wt% sample D.

From **Fig. 4.19**, it is clear that at lower than optimum injection rates, either one large wormhole or multiple wormholes were generated. At 0.5 cm^3/min, a conical wormhole was formed and face dissolution occurred for both 0.5 and 0.75 cm^3/min.

Fig. 4.19- Wormholes at the core inlet surfaces of the cores for injection rates of (left) 0.5 cm^3/min and (right) 0.75 cm^3/min.

When the injection rate was increased to the optimum, a single, dominant wormhole usually occurred. As the injection rate increased past the optimum, multiple wormholes were again generated. This is shown below in **Fig. 4.20**.

Fig. 4.20- Wormholes at the core inlet surface of the cores for an injection rate of (left) 2 cm^3/min and (right) 10 cm^3/min.

Decreasing the rate below the optimum rate, for example at 1.0 cm^3/min, did not create a significant amount face dissolution as HCl did, but it consumed 0.9 PV of acid, which is more than that at the optimum rate at 300°F. In the case of HCl, decreasing the

injection rate below the optimum increased the PV to breakthrough by an order of magnitude (Wang et al. 1993).

CT scans were performed on the two cores used in the experiments conducted at the highest and lowest injection rates (10 and 0.5 cm^3/min, respectively). **Fig. 4.21** shows the effect of injection rate on the wormhole size. At 0.5 cm^3/min, there is one large, dominant wormhole while at 10 cm^3/min, multiple branched wormholes were formed.

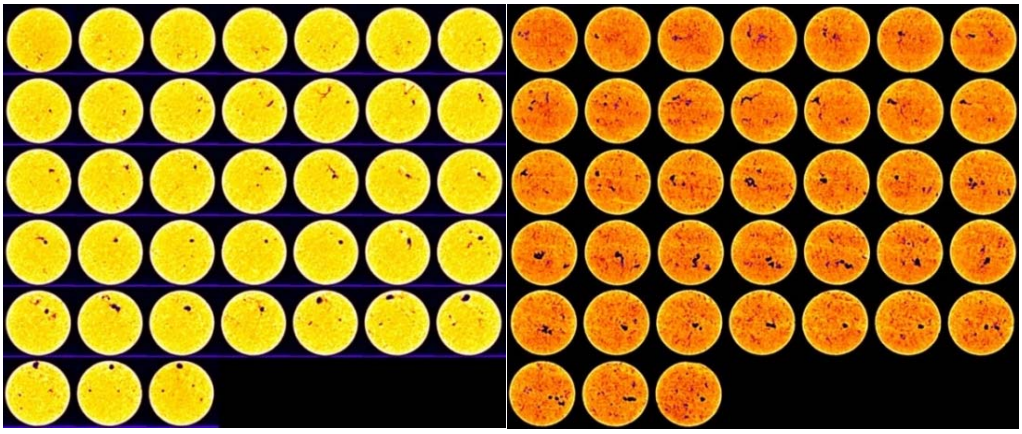

Fig. 4.21- Effect of injection rate on the size of propagating wormholes: (left) 0.5 cm^3/min and (right) 10 cm^3/min.

Conclusions

Coreflood tests were conducted using 6 in. long calcite cores and 10 wt% solutions of the new organic acid at 300°F. Based on the results obtained, the following conclusions can be drawn:

1. At 205°F, sample A created wormholes and achieved breakthrough in Indiana limestone cores. However, at 300°F, calcium phosphate precipitation occurred and acid breakthrough was not achieved.

2. At 300°F, samples B and D created wormholes and achieved breakthrough in Indiana limestone cores.
3. Sample D was chosen for the optimum injection rate investigation because it consumed less PV to breakthrough than sample B (5.59 compared to 11.96 PV)
4. The optimum injection rate for sample D was determined to be 2 cm^3/min.
5. The PV_{bt} vs. the injection rate behavior obtained in this study is similar to the results reported for 10 wt% Na_4EDTA at 250°F (Huang et al. 2003) and 20 wt% GLDA at 180°F (Mahmoud et al. 2011).

CHAPTER V

CONCLUSIONS AND RECOMMENDATIONS

The objective of this work was to evaluate the use of four samples of a newly developed organic acid as a stand-alone stimulation fluid for deep wells in carbonate reservoirs. In Chapter I, we showed the problems associated with HCl such as corrosion of well tubulars at high temperatures. To reduce this problem, numerous additives were required. Some reservoirs have low fracture pressure, and to avoid formation fracture during the acidizing treatment, HCl should be injected at low injection rates. However, this would cause face dissolution and would not bypass the damaged zone. In turn, this would not cause an increase in production.

In Chapter II, the rheological properties of the four new organic acid samples were measured. The samples had pH values between 0.59 and 1.84 and their measured density ranged between 1.075 and 1.151 g/cm^3. Using ICP-OES, sample A was found to contain 12,000 ppm of phosphorus which came from the use of phosphoric acid in the synthesis process. This finding would later explain the reduction in the reaction rate of this sample with calcite after increasing the temperature from 200 to 250°F. The viscosities of three of the samples were measured to be between 3.696 to 4.942 cP at room temperature. In addition, samples A and D of the organic acid (both at a concentration of 10 wt%) were titrated with 2.0 M NaOH to determine their respective molarities and molecular weights. Sample A was found to have a concentration of 1.324 M and a molecular weight of 392.86 g/gmol, while sample D had a concentration of 1.874 M and a molecular weight of 305.56 g/gmol. Also, sample A had two equivalence

points, indicating that it is a diprotic acid. Using the data from the titration test, the dissociation constants, K_{a1} and K_{a2}, were calculated to be 1.897×10^{-2} M and 9.015×10^{-8} M.

In Chapter III, the rotating disk apparatus (RDA) was used to conduct a detailed study of the reaction rate of the four samples of the new organic acid with calcite. Using sample A, the effects of temperature (150, 200, and 250°F) and disk rotational speed (100-1,700 rev/min) on the dissolution rate of calcite in the acid were examined in detail. At 150°F, the reaction was found to be controlled by mass transfer up to 500 rev/min, and by surface reaction afterwards. At 200°F, the reaction was mass transfer controlled for the entire range of rotational speeds that were examined. At 250°F, the reaction was mass transfer limited from 100-1,000 rev/min and then surface reaction controlled afterwards. However, all the dissolution rates at 250°F were lower than at 200°F. To explain this occurrence, XRF analysis was conducted on the surfaces of the cores used for these experiments and significant amounts of phosphorus were detected, indicating the presence of a calcium phosphate precipitate. Using the density and viscosity measurements from Chapter I, the diffusion coefficient of sample A was calculated for the three temperatures examined, and due to the precipitation problem, no Arrhenius relationship between temperature and diffusion coefficient could be established after 200°F. Afterwards, the remaining three samples of the acid were examined using RDA at a fixed rotational speed of 1,000 rev/min and temperatures of 200 and 250°F. At 200°F, all three samples had dissolution rates lower than sample A. In contrast to sample A, the

dissolution rate of calcite in samples B and D increased by increasing the temperature to 250°F.

In Chapter IV, the ability of three samples of the new organic acid to stimulate low-permeability Indiana limestone cores (1-10 md) was examined using the coreflood apparatus. At 200°F, sample A was used at an injection rate of 2 cm^3/min, and breakthrough was achieved after 6.6 PV of fluid were injected. At 300°F, however, the acid-rock reaction resulted in calcium phosphate precipitation and acid breakthrough was not achieved. SEM analysis confirmed the presence of phosphorus on the core surface and inside it. Then, the performance of samples B and D was evaluated at 300°F and an injection rate of 2 cm^3/min. Sample B achieved breakthrough after the injection of 11.9 PV as compared to only 5.59 PV of sample D for the same outcome. Due to its superior performance, sample D was chosen for the optimum injection rate investigation. To this effect, six more experiments were conducted using sample D at 300°F and at injection rates of 0.5, 0.75, 1, 3, 5, and 10 cm^3/min. As a result, it was determined that 2 cm^3/min was the optimum injection rate and that the PV_{bt} vs. injection rate behavior obtained is similar to the results reported for 10 wt% Na_4EDTA at 250°F (Huang et al. 2003) and 20 wt% GLDA at 180°F (Mahmoud et al. 2011).

Having evaluated the four samples of the new organic acid as stand-alone stimulation fluids, we recommend the following:

1. Sample A should not be used at temperatures greater than 200°F because its high phosphoric acid content results in calcium phosphate precipitation.

2. For high temperature reservoirs (>250°F), HCl will cause severe damage to the well completion (casing and production tubing). Therefore, sample D of the new organic acid should be used as an alternative.
3. Sample D can be used as an alternative to HCl at low injection rates to avert the problem of face dissolution caused by the latter.

Based on the above, any future research should be done using sample D as it was the most effective stimulation fluid of the four samples examined in this study. Finally, the following is a list that provides these topics:

1. The mass transfer and reaction kinetics of sample D with calcite should be examined in the same way those of sample A were.
2. The effects of salts on the dissolution rate should be investigated.
3. The effect of temperature on the optimum injection rate should be investigated.
4. The mass transfer and reaction kinetics of sample D with dolomite should be examined.
5. The effect of using dolomite on the optimum injection rate should be investigated.

REFERENCES

Alkattan, M., Oelkers, E., Dandurand, J., Schott, J., 1998. An Experimental Study of Calcite and Limestone Dissolution rates as a Function of pH from -1 to 3 and Temperature from 25 to 80 °C. *Chemical Geology* **151**(1-4): 199-214.

Al-Khaldi, M.H., Nasr-El-Din, H.A., Blauch, M.E., and Funkhouser, G.P. 2005. New Findings on Damage Potential, Geochemical Reaction Mechanisms, and Production Enhancement Applications for Citric Acid. *SPE J*. **10**(3): 267-275.

Al-Khaldi, M.H., Sarma, H., Nasr-El-Din, H.A. 2007. Reaction of Citric Acid with Calcite. *Chemical Engineering Science* 62(21): 5880-5896.

Al-Khaldi, M.H., Nasr-El-Din, H.A., Mehta, S., and Al-Aamri, A.D. 2010. Diffusivity of Citric Acid During its Reaction with Calcite. *JCPT* **49**(8): 43-52.

Almond, S.W., Harris, R.E., and Penny, G.S. 1995. Utilization of Biologically Generated Acid for Drilling Fluid Damage Removal and Uniform Acid Placement Across Long Formation Intervals. Paper SPE 30123 presented at the SPE European Formation Damage Conference, The Hague, Netherlands.

Barron, A.N., Hendrickson, A.R., and Wieland, D.R. 1962. The Effect of Flow on Acid Reactivity in a Carbonate Fracture. *Journal of Petroleum Technology* **14**(4):409-415.

Bazin, B., Roque, C. and Bouteca, M. 1995. A Laboratory Evaluation of Acid Propagation in Relation to Acid Fracturing: Results and Interpretation. Paper SPE 30085 presented at the European Formation Damage Conference, The Hague, Netherlands, 15-16 May. DOI: 10.2118/30085-MS.

Buijse, M., de Boe, P., Breukel, B., and Burgos, G. 2004. Organic Acids in Carbonate Acidizing. *SPE Prod & Fac* **19**(3): 128-134.

Burns, K.L. 2002. A Rotating Disk Study of the Mechanisms of Calcite Dissolution in the Presence of Environmentally Benign Polyaspartic Acid. Master Thesis, North Carolina State University.

Chatelain, J.C., Silberberg, I.H., Schechter, R.S. 1976. Thermodynamic Limitations in Organic Acid/Carbonate Systems. *SPE J.* **16**(4): 189-195.

Crowe, C.W., McGowan, G.R., Baranet, S.E. 1988. Investigation of Retarded Acids Provides Better Understanding of Their Effectiveness and Potential Benefits. Paper SPE 18222 presented at the SPE Annual Technical Conference and Exhibition, Houston, TX, 2-5 October.

Da Motta, E.P., Quiroga, M.H.V., Aragão, A.F.L., Pereira, A. 1998. Acidizing Gas Wells in the Merluza Field Using an Acetic/Formic Acid Mixture and Foam Pigs. Paper SPE 39424 presented at the SPE International Symposium on Formation Damage Control, Lafayette, LA, 18-19 February.

Daccord, G., 1987. Chemical dissolution of a porous medium by a reactive fluid. *Phys. Rev. Lett*., 58, 479.

Daccord, G., Leonormand, R. and Lietard, O. 1993a. Chemical Dissolution of a Porous Medium By A Reactive fluid-1. model for the "Wormholing" Phenomenon. *Chem. Eng. Sci.*, 48, 169.

Daccord, G., Leonormand, R. and Lietard, O. 1993b. Chemical Dissolution of a Porous Medium By A Reactive Fluid-2. Convection vs Reaction, Behavior Diagram. *Chem. Eng. Sci.*, 48, 179.

Ellison, B. T. 1969. Mass Transfer to a Rotating Disk. PhD Thesis University of California, Berkeley.

Fredd, C.N., 2000. Advances in Understanding and Predicting Wormhole Formation. Reservoir Stimulation. 3rd Edition. Wiley, New York. p. A16-1.

Fredd, C.N. and Fogler, H.S. 1998a. Alternative Stimulation Fluids and Their Impact on Carbonate Acidizing. *SPE J.* **3**(1): 34-41.

Fredd, C.N. and Fogler, H.S. 1998b. The Influence of Chelating Agents on the Kinetics of Calcite Dissolution. *Journal of Colloid and Interface Science* **204:** 187-197.

Fredd, C.N. and Fogler, H.S. 1998c. The Kinetics of Calcite Dissolution in Acetic Acid Solutions. *Chemical Engineering Science* **53**(22): 3863-3874.

Fredd, C.N. and Fogler, H.S. 1999. Optimum Conditions for Wormhole Formation in Carbonate Porous Media: Influence of Transport and Reaction. *SPE Journal*, **4**(3): 196-205. SPE-56995-PA. doi:10.2118/56995-PA.

Hansford, G.S. and Litt, M. 1968. Mass Transfer from a Rotating Disk to Power-Law Liquids. *Chemical Engineering Science* **23**(8): 849-864.

Harris, F.N. 1961. Application of Acetic Acid to Well Completion, Stimulation and Reconditioning. *Journal of Petroleum Technology* **13**(7): 637-639.

Hill, A.D. Zhu, D., and Wang, Y. 1995. The Effect of Wormholing on the Fluid-Loss Coefficient in Acid Fracturing. *SPE Prod & Fac* **10**(4): 257-26224. SPE-27403-PA. doi: 10.2118/27403-PA.

Hoefner, M. L. and H. S. Fogler, 1989. Fluid-Velocity and Reaction-Rate Effects During Carbonate Acidizing: Application of Network Model. *SPE Production Engineering*, 56-58.

Huang, T., Hill, A.D., and Schechter, R.S. 1997. Reaction Rate and Fluid Loss: The Keys to Wormhole Initiation and Propagation in Carbonate Acidizing. Paper SPE 37312 presented at the International Symposium on Oilfield Chemistry, Houston, 18-21 February. Doi: 10.2118/37312-MS.

Huang, T., Ostensen, L., Hill, A.D. 2000. Carbonate Matrix Acidizing with Acetic Acid. Paper SPE 58715 presented at the SPE International Symposium on Formation Damage Control, Lafayette, LA, 23-24 February.

Huang, T. McElfresh, P.M., and Garbrysch, A.D. 2003. Carbonate Acidizing Fluids at High Temperatures: Acetic Acid, Chelating Agents or Long-Chained Carboxylic Acids? Paper SPE 82268 presented at the SPE European Formation Damage Conference, The Hague, 13-14 May. doi: 10.2118/82268-MS.

Kung, M.S. 1998. Flow and reaction of weak acids in carbonate porous media. MS Thesis, University of Michigan, Ann Arbor, Michigan.

Levich, V.G. 1962. Physicochemical Hydrodynamics, Engelwood Cliffs, New Jersey, Prentice Hall.

Li, Y., Sullivan, R.B., de Rozieres, J., Gaz, G.L., and Hinkel, J.J. 1993. An Overview of Current Acid Fracturing Technology With Recent Implications for Emulsified Acids. Paper SPE 26581 presented at the SPE Annual Technical Conference and Exhibition, Houston, 3-6 October.

Lund, K., Fogler, H.S., McCune, C.C., and Ault, J.W. 1973. Acidization- I. The Dissolution of Dolomite in Hydrochloric Acid. *Chemical Engineering Science* **28**(3): 691-700.

Lund, K., Fogler, H.S., McCune, C.C., and Ault, J.W. 1975. Acidization- II. The Dissolution of Calcite in Hydrochloric Acid. *Chemical Engineering Science* **30**(8): 825-835.

Mahmoud, M.A., Nasr-El-Din, H.A., De Wolf, C.A., and LePage, J.N. 2010a. Evaluation of a New Environmentally Friendly Chelating Agent for High Temperature Applications. Paper SPE 127923 presented at the SPE International Symposium and Exhibition on Formation Damage Control, Lafayette, Louisiana, USA. 10-12 February. doi: 10.2118/127923-MS.

Mahmoud, M.A., Nasr-El-Din, H.A., De Wolf, C.A., and LePage, J.N. 2010b. An Effective Stimulation Fluid for Deep Carbonate Reservoirs: A Core Flood Study. Paper SPE 131626 presented at the International Oil and Gas Conference and Exhibition in Beijing, China, 8-10 June. doi: 10.2118/131626-MS.

Mahmoud, M.A., Nasr-El-Din, H.A., De Wolf, C.A., and LePage, J.N. 2011. Optimum Injection Rate of a New Chelate That Can Be Used To Stimulate Carbonate Reservoirs. *SPE J.* **16**(4): 968-980.

Nasr-El-Din, H.A., Lynn, J.D., Taylor, K.C. 2001. Lab Testing and Field Application of a Large Scale Acetic-Based Treatment in a Newly Developed Carbonate Reservoir. Paper SPE 65036 presented at the SPE International Symposium on Oilfield Chemistry, Houston, TX, 23-16 February.

Newman, J. 1966. Schmidt Number Correction for the Rotating Disk. *J. of Physical Chemistry*, **70**(4): 1327-1328.

Nierode, D.E. and Williams, B.B. 1971. Characteristics of Acid Reaction in Limestone Formations. *SPE J*. **11**(4): 406-418.

Still, J.W., Dismuke, K., and Frenier, W.W. 2007. Generating Acid Downhole in Acid Fracturing. U.S. Patent No. 7166560.

Talbot, M. S. and R. D. Gdanski, 2008. Beyond the Damköhler Nuber: A New Interpretation of Carbonate Wormholing. Paper SPE 113042 presented at the SPE Europec/EAGE Annual Conference and Exhibition, 9-12 June. 10.2118/113042-MS.

Taylor, K.C. Al-Ghamdi, A.H. and Nasr-El-Din, H.A. 2004. Effect of Additives on the Acid Dissolution Rates of Calcium and Magnesium Carbonates. *SPE J.* **19**(3): 122-127.

Van Domelen, M.S., Jennings, A.R. 1995. Alternate Acid Blends for HPHT Applications. Paper SPE 30419 presented at the SPE Offshore Europe Conference, Aberdeen, Scotland, 5-8 September.

Wang, X., Qu, Q., Cutler, J., and Boles, J.L. 2009. Nonaggressive Matrix Stimulation Fluids for Simulataneous Stimulation of Heterogeneous Carbonate Formations. Paper SPE 121712 presented at the SPE International Symposium on Oilfield Chemistry, The Woodlands, Texas, USA, 20-22 April. doi: 10.2118/121712-MS.

Wang, Y., Hill, A.D., and Schechter, R.S. 1993. The Optimum Injection Rate for Matrix Acidizing of Carbonate Formations. Paper SPE 26578 presented at the SPE Annul

Technical Conference and Exhibition, Houston, Texas, 3-6 October. doi: 10.2118/26578-MS.

Williams, B., Gidley, J. and Schechter, R.S. 1979. Acidizing Fundamentals, Richardson: SPE Monograph Series.